Neuron

Article

Anterior cingulate cortex projections to the dorsal medial striatum underlie insomnia associated with chronic pain

Graphical abstract

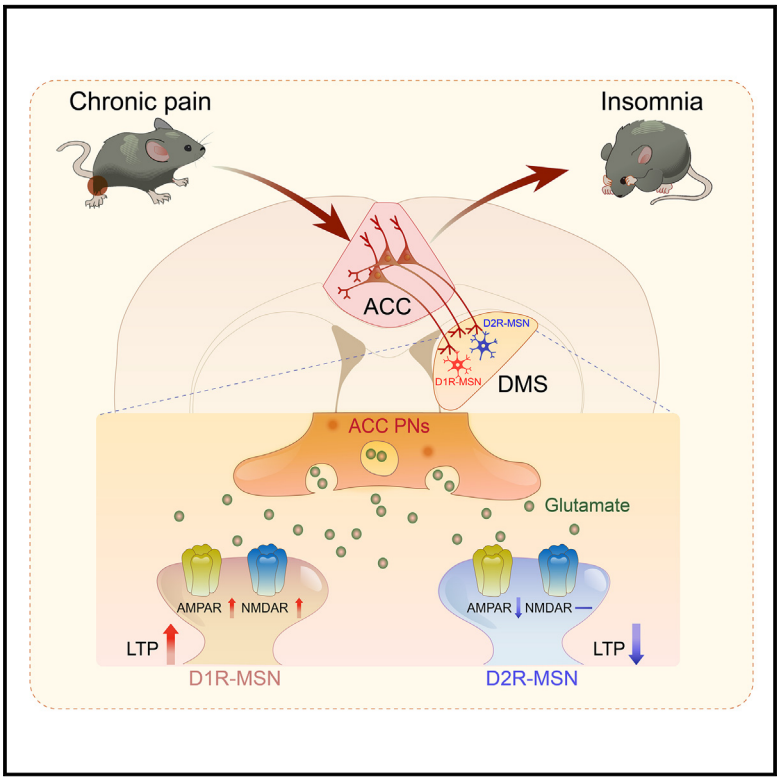

Highlights

- ACC pyramidal neurons (PNs) are selectively activated during chronic-pain-induced insomnia
- Lesion of ACC PNs abolishes chronic-pain-induced insomnia
- Hyperactive ACC PNs control chronic-pain-induced insomnia via the DMS pathway
- Enhanced plasticity of ACC PNs to DMS D1R-MSNs mediates insomnia

Authors

Ya-Dong Li, Yan-Jia Luo, Wei-Kun Su, ..., Zi-Long Liu, Wei-Min Qu, Zhi-Li Huang

Correspondence

yadlee@126.com (Y.-D.L.), liu.zilong@zs-hospital.sh.cn (Z.-L.L.), quweimin@fudan.edu.cn (W.-M.Q.), huangzl@fudan.edu.cn (Z.-L.H.)

In brief

Over 50% of chronic pain patients experience insomnia. Li et al. reveal that heightened activity of anterior cingulate cortex excitatory neurons precisely governs chronic-pain-induced insomnia via the dorsal medial striatum pathway. This effect relies on enhanced plasticity in dopamine D1-receptor-positive medium spiny neurons.

Li et al., 2024, Neuron *112*, 1–14
April 17, 2024
https://doi.org/10.1016/j.neuron.2024.01.014

CellPress

Neuron

CellPress

Article

Anterior cingulate cortex projections to the dorsal medial striatum underlie insomnia associated with chronic pain

Ya-Dong Li,[1,2,7,8,*] Yan-Jia Luo,[1,3,7] Wei-Kun Su,[2,7] Jing Ge,[1] Andrew Crowther,[4] Ze-Ka Chen,[1] Lu Wang,[1] Michael Lazarus,[5] Zi-Long Liu,[1,6,*] Wei-Min Qu,[1,*] and Zhi-Li Huang[1,*]

[1]Department of Pharmacology, School of Basic Medical Sciences, State Key Laboratory of Medical Neurobiology, Institutes of Brain Science and Collaborative Innovation Center for Brain Science, Joint International Research Laboratory of Sleep, and Department of Anesthesiology, Zhongshan Hospital, Fudan University, Shanghai 200032, China

[2]Songjiang Research Institute, Songjiang Hospital affiliated to Shanghai Jiao Tong University School of Medicine, Shanghai Key Laboratory of Emotions and Affective Disorders (LEAD), Shanghai 201699, China

[3]Department of Anesthesiology, Shanghai Ninth People's Hospital, Shanghai Jiao Tong University School of Medicine, Shanghai 200011, China

[4]Department of Anatomy, University of California, San Francisco, San Francisco, CA 94158, USA

[5]International Institute for Integrative Sleep Medicine (WPI-IIIS) and Institute of Medicine, University of Tsukuba, 1-1-1 Tennodai, Tsukuba, Ibaraki 305-8575, Japan

[6]Department of Pulmonary Medicine, Zhongshan Hospital, Fudan University, Shanghai 200032, China

[7]These authors contributed equally

[8]Lead contact

*Correspondence: yadlee@126.com (Y.-D.L.), liu.zilong@zs-hospital.sh.cn (Z.-L.L.), quweimin@fudan.edu.cn (W.-M.Q.), huangzl@fudan.edu.cn (Z.-L.H.)

https://doi.org/10.1016/j.neuron.2024.01.014

SUMMARY

Chronic pain often leads to the development of sleep disturbances. However, the precise neural circuit mechanisms responsible for sleep disorders in chronic pain have remained largely unknown. Here, we present compelling evidence that hyperactivity of pyramidal neurons (PNs) in the anterior cingulate cortex (ACC) drives insomnia in a mouse model of nerve-injury-induced chronic pain. After nerve injury, ACC PNs displayed spontaneous hyperactivity selectively in periods of insomnia. We then show that ACC PNs were both necessary for developing chronic-pain-induced insomnia and sufficient to mimic sleep loss in naive mice. Importantly, combining optogenetics and electrophysiological recordings, we found that the ACC projection to the dorsal medial striatum (DMS) underlies chronic-pain-induced insomnia through enhanced activity and plasticity of ACC-DMS dopamine D1R neuron synapses. Our findings shed light on the pivotal role of ACC PNs in developing chronic-pain-induced sleep disorders.

INTRODUCTION

Approximately 20% of the general population suffers from chronic pain,[1] with significant comorbidity of depression,[2–4] poor memory,[5,6] and sleep disturbance.[7,8] Sleep complaints are present in 67%–88% of chronic pain patients, and at least 50% meet the criteria for insomnia.[9] Chronic-pain-induced insomnia not only intensifies pain but also impairs memory[10,11] and increases the risk of depression,[12] highlighting the need to address this comorbidity to improve overall patient outcomes. Despite the significant impact of chronic-pain-induced insomnia on patients, there has been limited research exploring the neuronal circuits underlying this phenomenon. Additionally, it remains unclear how the sleep-wake regulating circuits are affected by chronic pain and further mediate insomnia.

As the input of basal ganglia, the dorsal medial striatum (DMS) plays a key role in sleep-wake regulation.[13–15] The two distinct populations of neurons play opposite roles in sleep-wake control: dopamine D1 receptor (D1R)-expressing medium spiny neurons (MSNs) promote wakefulness,[14] whereas dopamine D2 receptor (D2R)-MSNs promote sleep.[15] Interestingly, as one of the major inputs to the DMS, the anterior cingulate cortex (ACC) is reliably activated in chronic pain models and necessary for the processing of pain affect.[16–18] Pyramidal neurons (PNs) within the ACC have been shown to control features of mechanical allodynia in neuropathic pain models.[19] Besides, optogenetic activation of ACC corticospinal projections results in mechanical hypersensitivity, whereas inhibition produces acute analgesia.[20] Although the ACC was not treated as a wake-promoting center, recent evidence indicates that the ACC is involved in modulating

Please cite this article in press as: Li et al., Anterior cingulate cortex projections to the dorsal medial striatum underlie insomnia associated with chronic pain, Neuron (2024), https://doi.org/10.1016/j.neuron.2024.01.014

wakefulness within specific contexts, such as a novel environment[21] and depression,[22] suggesting that heightened activity among ACC PNs may contribute to insomnia associated with chronic pain. However, whether the ACC-DMS circuit is involved in chronic-pain-induced insomnia and how chronic pain reshapes ACC PNs to DMS MSNs projections are unknown. We hypothesized that ACC PNs control chronic-pain-induced insomnia through enhanced synaptic connections to DMS D1R-MSNs.

To test our hypothesis, we conduct imaging studies in live animals and confirm that hyperactivity of ACC PNs is mainly associated with insomnia in chronic pain mice caused by nerve injury. Next, through gain- and loss-of-function experiments, we establish that ACC PNs play a causal role in regulating chronic-pain-induced insomnia through the ACC-DMS pathway. Using optogenetics-assisted slice electrophysiology, we further examine the synaptic plasticity of ACC-DMS D1R-MSNs/D2R-MSNs synapses following nerve injury. We find that the chronic-pain-induced hyperactivity of ACC PNs is reflected in the synaptic dynamics of D1R-MSNs rather than D2R-MSNs. Lastly, inhibition of DMS D1R-MSNs reverses chronic-pain-induced insomnia. Collectively, these studies demonstrate that the ACC PNs underlie insomnia associated with chronic neuropathic pain conditions, highlighting the ACC PN-DMS pathway as a potential target for therapeutic interventions aimed at addressing insomnia associated with chronic pain.

RESULTS

Aberrant activation of ACC PNs in chronic-pain-induced insomnia

To establish the presence of chronic-pain-induced sleep disorders, we initially assessed the quantity of sleep-wake patterns in a mouse model of neuropathic pain induced by partial sciatic nerve ligation (PSNL) (Figures S1A–S1C). The PSNL model is widely recognized as a reliable and established method for inducing chronic pain and subsequent insomnia, as demonstrated in our previous studies.[23–25] In this study, we observed a significant increase in wakefulness during ZT0–ZT2 (07:00–09:00) in PSNL mice compared with the sham group (Figures S1D and S1E). Conversely, the sham mice exhibited a shorter latency to non-rapid eye movement (NREM) sleep onset and a longer mean duration of NREM sleep, without a difference in electroencephalogram (EEG) power density or episode number of NREM sleep during this time period (Figures S1F–S1J). These results confirm sleep disorders in PSNL mice.

Using *in vivo* calcium imaging and c-Fos labeling, previous studies reported that ACC PNs are activated in mice with chronic pain,[16,17,26] but it is unclear whether ACC PNs are selectively activated in chronic-pain-induced insomnia. Initially, we recorded the dynamic calcium activity of ACC PNs during two specific time intervals, ZT0–ZT2 (07:00–09:00) and ZT12–ZT14 (19:00–21:00), prior to PSNL surgery (refer to "base"). Subsequently, PSNL was applied to these mice, and after a 7-day period, we recorded the calcium activity of ACC PNs again at the same time points (refer to "PSNL," Figures 1A–1C; Video S1). To investigate whether ACC PNs are specifically active due to chronic pain or chronic-pain-induced insomnia, we chose the time intervals of 07:00–09:00, corresponding to the insomnia phase in PSNL mice, and 19:00–21:00, when both naive and PSNL mice are awake (Figure S1D). Interestingly, we observed an increase in the calcium activity of ACC PNs only during the insomnia phase (07:00–09:00), not during the physiologically active phase (19:00–21:00), when compared with naive mice (Figures 1D and 1E). Furthermore, during sleep loss in the light phase, we noted that a substantial portion (62%) of ACC PNs show elevated calcium activity compared with their activity before PSNL surgery (Figure 1F). In contrast, during the initial 2 h of the dark phase when both sham and PSNL mice were awake, only 21% of ACC PNs in PSNL mice exhibited increased calcium activity (Figure 1F). These findings suggest that ACC PNs are abnormally activated specifically during chronic-pain-induced insomnia in PSNL mice.

To further affirm the selective activation of ACC PNs by chronic-pain-induced insomnia, we examined whether the ACC PNs' activity remained elevated when exposed to hypnotics (diazepam), analgesics (morphine), or a combined analgesic and hypnotic compound (gabapentin) (Figures 1G and 1H). Initially, we established that there are more active ACC PNs in chronic-pain-induced insomnia mice (PSNL) compared with naive mice (base, Figure 1I). Interestingly, we found that treatment with either diazepam or morphine did not significantly decrease the number of active PNs in the ACC compared with chronic-pain-induced insomnia mice (PSNL) without drug treatment (Figure 1I). Remarkably, gabapentin treatment significantly decreased the number of active PNs in the ACC, comparable to the levels observed in naive mice (Figure 1I). We further assessed the calcium activity of single-unit ACC PNs during chronic-pain-induced insomnia (PSNL) and after treatment with diazepam, morphine, or gabapentin (Figure 1J). Consistently, the calcium activity of ACC PNs was only reduced by gabapentin treatment (Figure 1K). These results provide additional evidence supporting the notion that ACC PNs are specifically activated by chronic-pain-induced insomnia.

To investigate the aberrant activity of ACC PNs, we conducted electrophysiological recordings to examine the excitatory inputs to ACC PNs. ACC PNs were labeled by injecting AAV-DIO-mCherry into the ACC of CaMKII-Cre mice (Figures S2A and S2B). Acute brain tissues were collected during 07:00–09:00 and 19:00–21:00 in both PSNL and sham mice to align with the conducted calcium imaging procedures. Remarkably, we observed a significant increase in the frequency, but not the amplitude, of miniature excitatory postsynaptic currents (mEPSCs) in ACC PNs from brain tissues collected during 07:00–09:00 in PSNL mice (Figures S2C–S2E) compared with sham mice. However, there was no such difference observed during 19:00–21:00 (Figures S2F–S2H). These findings suggest an elevated presynaptic excitatory input to ACC PNs specifically during chronic-pain-induced insomnia. Taken together, these results show that the hyperactivity of ACC PNs is selectively related to chronic-pain-induced insomnia.

ACC PNs are required for chronic-pain-induced insomnia

Although the correlation of hyperactivity of ACC PNs and chronic-pain-induced insomnia has been indicated by *in vivo*

Please cite this article in press as: Li et al., Anterior cingulate cortex projections to the dorsal medial striatum underlie insomnia associated with chronic pain, Neuron (2024), https://doi.org/10.1016/j.neuron.2024.01.014

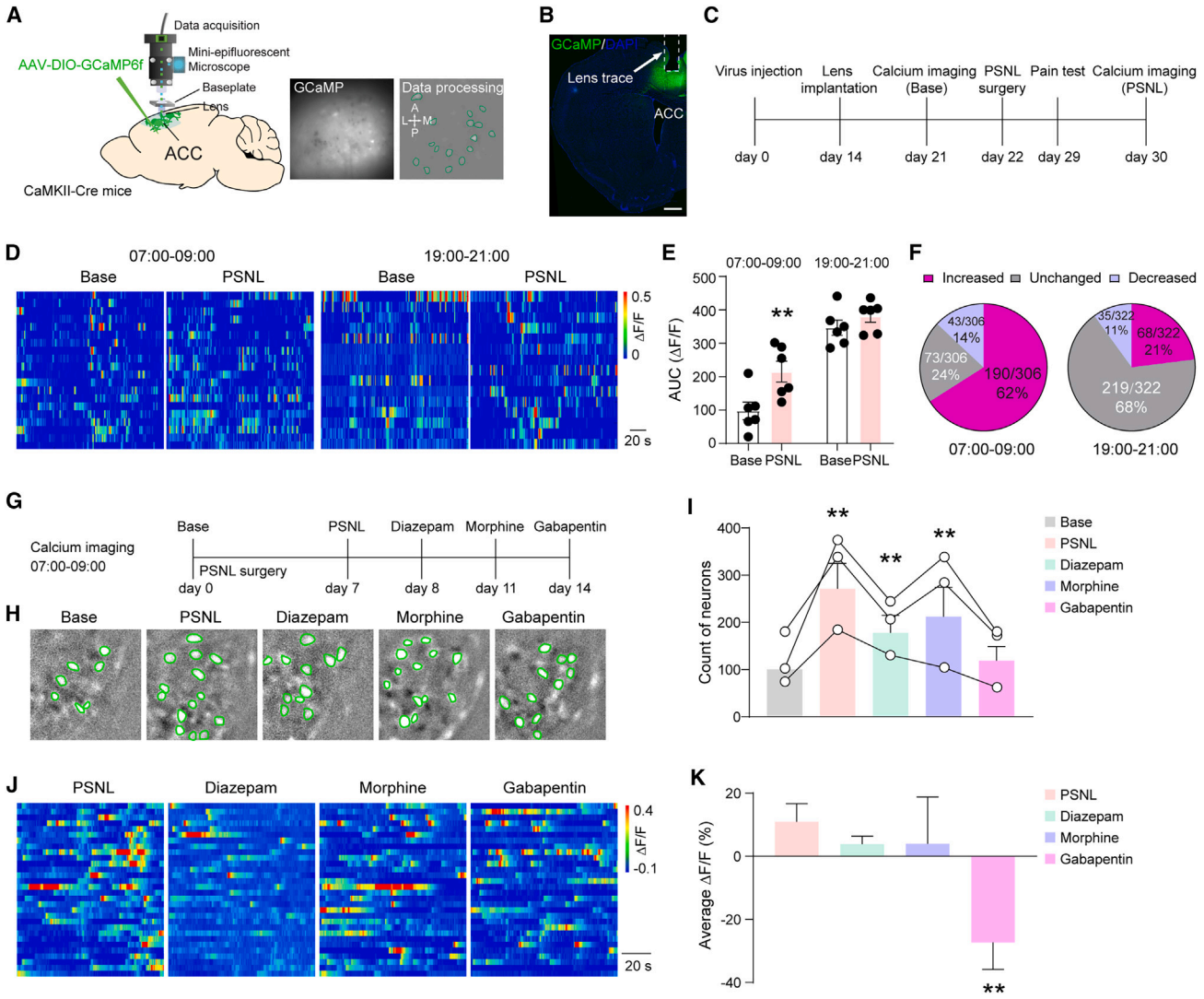

Figure 1. Aberrant activation of ACC PNs was associated with insomnia in PSNL mice

(A) Left: schematic diagram of calcium imaging of ACC PNs. AAV-DIO-GCaMP6f was injected into the unilateral ACC in CaMKII-Cre mice, followed by gradient refractive index (GRIN) lens and baseplate implantation. Right: an example raw image of GCaMP fluorescence and post-processing for calcium transient analysis.

(B) A representative image of GCaMP expression in the ACC with GRIN lens trace (indicated by the white arrow). Scale bars, 200 μm.

(C) Diagram of experimental design. Calcium activity of ACC PNs was recorded in naive mice (base) and 7 days after PSNL from the same mice from 07:00 to 09:00 and 19:00 to 21:00.

(D) Heatmap of calcium activity of single-unit ACC PNs at base and after PSNL. Calcium activity was recorded from 07:00 to 09:00 and 19:00 to 21:00.

(E) Quantification of the area under the curve (AUC) of calcium activity from 07:00 to 09:00 and 19:00 to 21:00. n = 6 mice, $^{**}p < 0.01$, two-way ANOVA followed by Tukey post hoc test.

(F) Proportion of ACC PNs pertaining to each category from all recorded animals in the first 2 h after light on (07:00–09:00) and light off (19:00–21:00). From 6 mice, a total of 306 cells were identified in the light phase and 322 cells were identified in the dark phase.

(G) Diagram of experimental design. Calcium activity of ACC PNs was recorded in naive mice (base) and the same mice 7 days after PSNL surgery from 07:00 to 09:00. Drug administration was given at 06:30.

(H) Example raw images of GCaMP fluorescence showed activation of PNs (green circles) in the ACC after drug treatments in PSNL mice.

(I) Quantification of cell counts of active PNs in the ACC after drug treatments in PSNL mice. n = 3 mice, $^{**}p < 0.01$, one-way ANOVA followed by Dunnett's t test for post hoc comparisons.

(J) Heatmap of calcium activity of single-unit ACC PNs identified during chronic-pain-induced insomnia and following drug treatments. Calcium activity of 30 PNs was recorded from 07:00 to 09:00 in PSNL mice.

(K) Average calcium activity of PNs during chronic-pain-induced insomnia and following drug treatments. $^{**}p < 0.01$, one-way ANOVA followed by Dunnett's t test for post hoc comparisons.

Data are shown as mean ± SEM. See also Figures S1 and S2 and Video S1.

Please cite this article in press as: Li et al., Anterior cingulate cortex projections to the dorsal medial striatum underlie insomnia associated with chronic pain, Neuron (2024), https://doi.org/10.1016/j.neuron.2024.01.014

calcium imaging, the causal role is unclear. To demonstrate the necessity of ACC PNs in chronic-pain-induced insomnia, we ablated ACC PNs by cell-type-specific caspase-3 expression. AAV-hSyn-DIO-caspase-3 (mixed with AAV-hSyn-DIO-EGFP) was injected into the ACC of CaMKII-Cre mice, and AAV-hSyn-DIO-EGFP was injected as the control (Figure 2A). GFP-positive neurons were ablated in the ACC by caspase-3 (Figure 2B). Von Frey mechanical thresholds and sleep duration were assessed 3 weeks after virus injection in pain-free (naive) mice, prior to the application of PSNL in both GFP-control and caspase-3 mice. 1 week after PSNL, the same GFP-control and caspase-3 mice were re-evaluated for mechanical thresholds and sleep duration. The ablation of ACC PNs only resulted in elevated hind paw withdrawal thresholds in mice subjected to PSNL, but not in naive mice (Figure 2C). Importantly, the mechanical pain thresholds in PSNL mice with ACC PN ablation only showed a partial restoration toward baseline levels, suggesting that the elimination of ACC PNs relieved, but did not completely alleviate, mechanical allodynia in PSNL mice. Strikingly, EEG/electromyogram (EMG) recordings showed that ablation of ACC PNs completely abolished chronic-pain-induced insomnia in PSNL mice, decreasing the time of wakefulness in the first 2 h after light on (ZT0–ZT2), 12-h (ZT0–ZT12) and 24-h periods (ZT0–ZT24), and increasing NREM sleep for 2 and 24 h (ZT0–ZT24) after light on (Figures 2D and 2F). Interestingly, lesions of ACC PNs slightly decreased wakefulness in the dark phase of naive mice (Figures 2E and 2F), suggesting that ACC PNs may be involved in maintaining wakefulness. Surprisingly, unilateral lesion of ACC PNs, either contralateral or ipsilateral to sciatic nerve ligation, only resulted in a partial alleviation of insomnia in PSNL mice (Figure S3), probably due to diverse input pathways to the bilateral ACC. Taken together, these results show that chronic-pain-induced sleep loss may rely on ACC PNs in PSNL mice.

Activation of ACC PNs is sufficient to induce sleep loss in naive mice

To further explore the causal role of hyperactivity of ACC PNs and chronic-pain-induced sleep disorders, we employed chemogenetics to mimic the aberrant activation of ACC PNs after PSNL. AAV-hSyn-DIO-hM3Dq-mCherry was bilaterally injected into the ACC of CaMKII-Cre naive (pain-free) mice (Figures 3A and 3B). Chemogenetic activation was validated by c-Fos labeling (Figure 3C). Activation of ACC PNs by clozapine-N-oxide (CNO) administration only slightly decreased mechanical pain thresholds, without a statistical significance ($p = 0.10$, Figure 3D), but significantly increased wakefulness for 4 h in CaMKII-Cre naive mice (Figures 3E–3G). Specifically, chemogenetic activation of ACC PNs induced an 85.5% increase in wakefulness and a 52.4% decrease in NREM sleep (07:00–11:00, Figures 3F and 3G), mimicking the difficulty of falling asleep in chronic pain mice. EEG power spectra of NREM sleep showed no difference in EEG power in NREM sleep or wakefulness from 07:00 to 11:00 (Figures 3H and 3I). As a control, chemogenetic activation of ACC PNs in the dark phase only slightly increased time of wakefulness when mice are physiologically awake (Figures S4A–S4C), suggesting that activation of ACC PNs does not robustly promote wakefulness in the dark phase. The same dosage of CNO (1 mg/kg) treatment in mCherry control mice did not change mechanical pain thresholds or sleep (Figures S4D–S4F). These results indicate that activation of ACC PNs in naive mice mimics chronic-pain-induced insomnia but not allodynia.

Taken together, the hyperactivity of ACC PNs plays a key role in controlling chronic-pain-induced insomnia in PSNL mice.

Hyperactivity of ACC PNs increases wakefulness through the DMS pathway

The ACC is not treated as a dominant sleep-wake regulation region; thus, it is unclear how hyperactivity of ACC PNs induced insomnia in chronic pain. The most intense output of ACC PNs is the DMS, which plays a curial role in sleep-wake regulation.[14,15] To confirm the functional connection of ACC PNs and DMS neurons, we optogenetically mapped ACC-DMS connections by electrophysiological recordings in brain slices of CaMKII-Cre mice (Figure S5A). Optogenetic stimulation of terminals of ACC PNs was applied in the DMS and responses from DMS neurons were recorded. The DMS neurons displayed typical morphology and electrophysiological properties of MSNs (Figures S5B and S5C). In total, 26 DMS MSNs were recorded and all neurons responded to blue light stimulation with spikes in the cell-attached mode (Figure S5D). The light-evoked EPSCs were blocked by α-amino-3-hydroxy-5-methyl-4-isoxazolepropionic acid receptor (AMPAR) antagonist NBQX and N-methyl-D-aspartate receptor (NMDAR) antagonist APV (Figure S5E). The mean latency was less than 5 ms (Figure S5F), indicating direct excitatory connections between ACC PNs and DMS MSNs.

To elucidate the ACC-DMS circuit in mediating wakefulness, we optogenetically stimulated the ACC-DMS pathway *in vivo* (Figures 4A and 4B). Optogenetic activation of ACC-DMS projections slightly decreased mechanical pain thresholds without statistical difference in naive mice (Figure 4C). However, blue light stimulation in the DMS frequency- and latency-dependently induced transitions from NREM sleep to wakefulness, while no significant changes were observed following yellow light stimulation as a control (Figures 4D and 4E). Chronic stimulation of the ACC-DMS circuit for 1 h (10 s ON/20 s OFF for 120 cycles) increased time of wakefulness by 280%, while NREM and REM sleep were decreased compared with yellow light controls (Figures 4F and 4G). Opto-stimulation in mCherry control mice did not change mechanical pain thresholds or sleep (Figures S4G–S4I). In addition to ACC-DMS projections, ACC-nucleus accumbens (NAc) projections are implicated in the regulation of chronic pain.[26] Nevertheless, optogenetic stimulation of ACC-NAc projections did not induce wakefulness (Figures S6).

To demonstrate the necessity of ACC-DMS projections in controlling chronic-pain-induced insomnia, we selectively inhibited DMS-projecting ACC neurons by chemogenetics in PSNL mice (Figures 4H and 4I). Chemogenetic inhibition of DMS-projecting ACC neurons was validated by c-Fos labeling (Figures 4J and 4K). Strikingly, inhibition of DMS-projecting ACC neurons restored sleep loss and increased mean duration of NREM sleep in PSNL mice (Figures 4L–4N), but only slightly increased mechanical pain thresholds in PSNL mice (Figure 4O), without affecting locomotion (Figure 4P). These results indicate that hyperactivity of DMS-projecting ACC neurons induces insomnia in PSNL mice.

Please cite this article in press as: Li et al., Anterior cingulate cortex projections to the dorsal medial striatum underlie insomnia associated with chronic pain, Neuron (2024), https://doi.org/10.1016/j.neuron.2024.01.014

CellPress

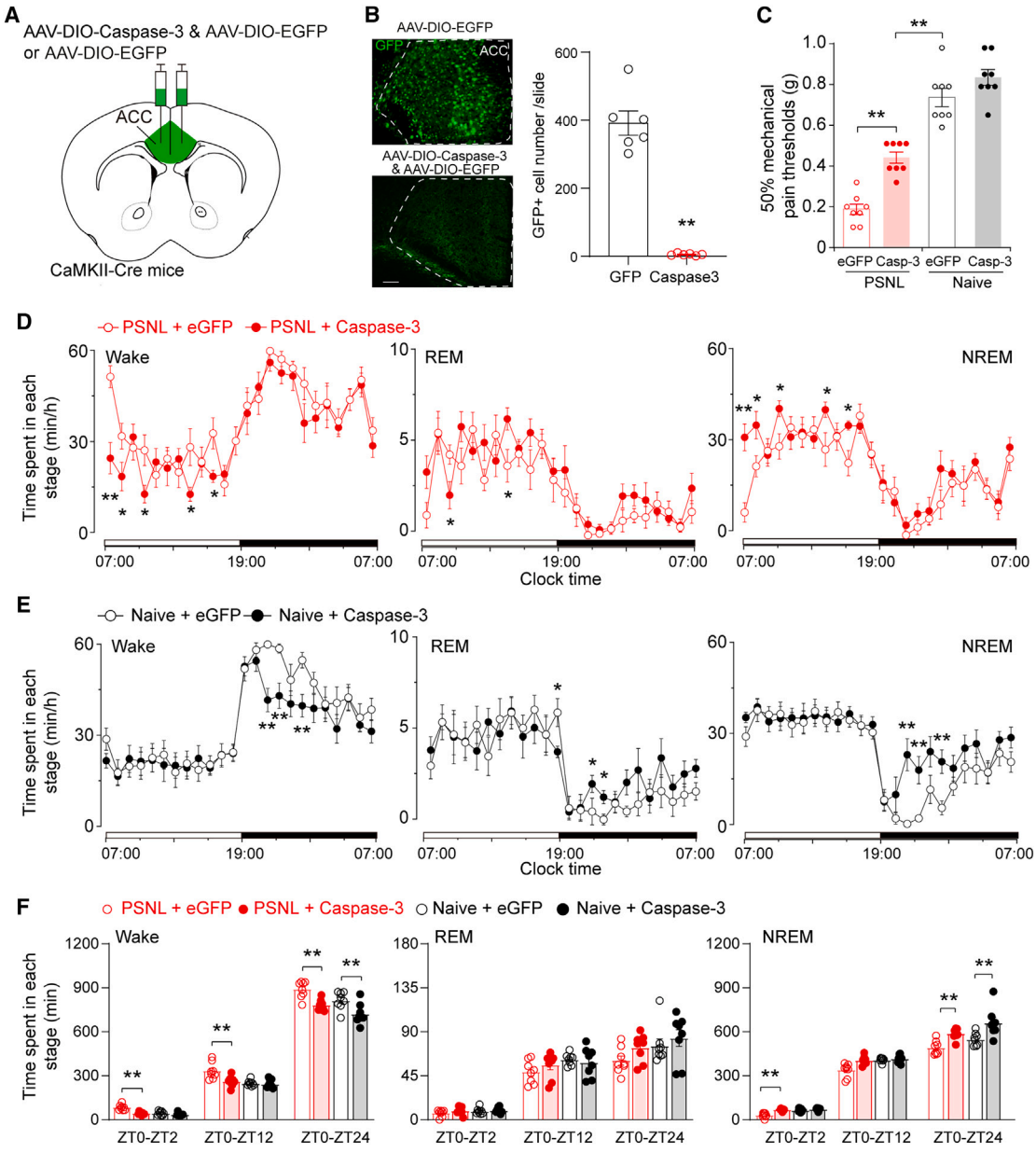

Figure 2. Ablation of ACC PNs abolished chronic-pain-induced insomnia in PSNL mice

(A) Schematic diagram of cell-type-specific lesion of ACC PNs. AAV-DIO-caspase-3/AAV-DIO-EGFP was bilaterally injected into the ACC in CaMKII-Cre mice.

(B) GFP+ cells were ablated in the ACC by caspase-3 expression. Sample images showing GFP+ cells in the ACC from a control or a caspase-3-treated mouse. Scale bars, 100 μm. n = 6 mice for each group, using unpaired t test.

(C) Mechanical pain thresholds after lesion of ACC PNs in PSNL and naive mice. n = 8 mice for each group, using two-way ANOVA, followed by Tukey post hoc test.

(D) Time course changes in wakefulness, REM, and NREM sleep after lesion of ACC PNs in PSNL mice. The horizontal filled bars on the x axis (clock time) indicate the 12-h dark periods. n = 8 mice for each group, using repeated-measures ANOVA, followed by Tukey post hoc test.

(E) Time course changes in wakefulness, REM, and NREM sleep after lesion of ACC PNs in naive mice. n = 8 mice for each group, using repeated-measures ANOVA, followed by Tukey post hoc test.

(F) Total time spent in each stage for ZT0–ZT2, ZT0–ZT12, and ZT0–ZT24 after lesion of ACC PNs. n = 8 mice for each group, using two-way ANOVA, followed by Tukey post hoc test.

Data are shown as mean ± SEM, *p < 0.05, **p < 0.01. See also Figure S3.

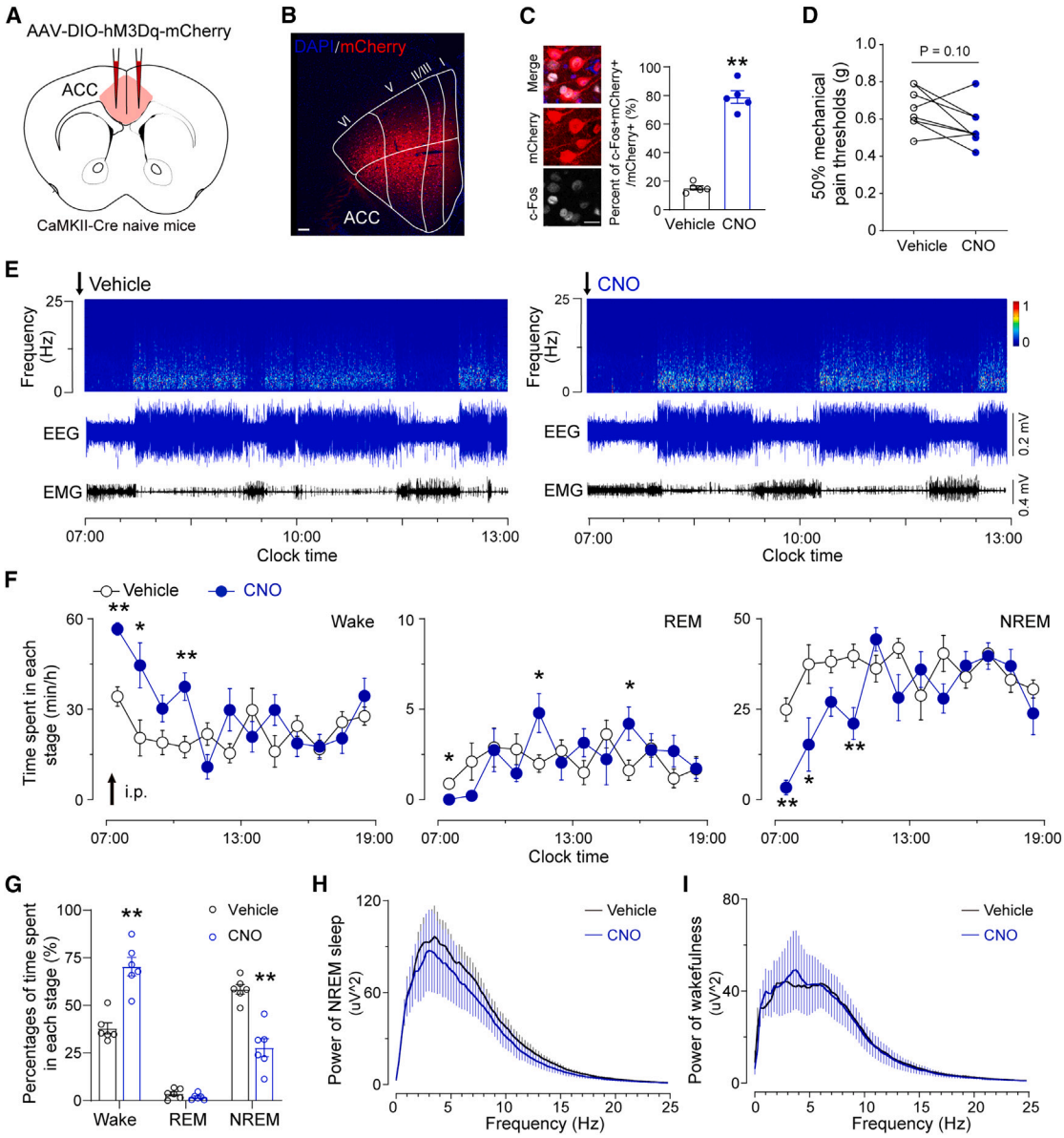

Figure 3. Chemogenetic activation of ACC PNs induced sleep loss

(A) Diagram of chemogenetic activation of ACC PNs. AAV-DIO-hM3Dq-mCherry was bilaterally injected into the ACC in CaMKII-Cre mice.

(B) An enlarged image showed that mCherry-positive cells are mostly located in layer II/III and layer V of the ACC. Scale bars, 100 μm.

(C) Representative images and quantification of c-Fos expression in ACC PNs 90 min after vehicle or CNO injection. Scale bars, 20 μm. n = 5 mice from each group, unpaired t test.

(D) Mechanical pain thresholds after activation of ACC PNs in naive mice. Von Fery tests were performed 30–60 min after vehicle or CNO administration. n = 8 mice, paired t test.

(E) Examples of relative EEG power and EEG/EMG traces following vehicle (left) or CNO (right) injection at 06:50.

(F) Time courses of wakefulness, REM, and NREM sleep after vehicle or CNO injection in naive mice. n = 6 mice, using repeated-measures ANOVA, followed by Tukey post hoc test.

(G) Percent of time spent in each stage for 4 h (07:00–11:00) after vehicle or CNO injection. n = 6 mice, paired t test.

(H and I) EEG power spectrum of NREM sleep (H) and wakefulness (I) during the 4 h after vehicle or CNO injection. Data are shown as mean ± SEM, *p < 0.05, **p < 0.01. See also Figure S4.

Increased excitability of DMS D1R-MSNs in chronic pain

In the DMS, two distinct populations of MSNs, namely the D1R-MSNs and D2R-MSNs, control arousal and sleep, respectively.[14,15] To explore how DMS MSNs mediate chronic-pain-induced insomnia, we measured the activity and synaptic plasticity of DMS D1R-MSNs and D2R-MSNs in chronic pain mice by *in vitro* electrophysiologic recording. We subjected transgenic mice expressing GFP in D2R-MSNs (D2R-EGFP mice) to

Please cite this article in press as: Li et al., Anterior cingulate cortex projections to the dorsal medial striatum underlie insomnia associated with chronic pain, Neuron (2024), https://doi.org/10.1016/j.neuron.2024.01.014

CellPress

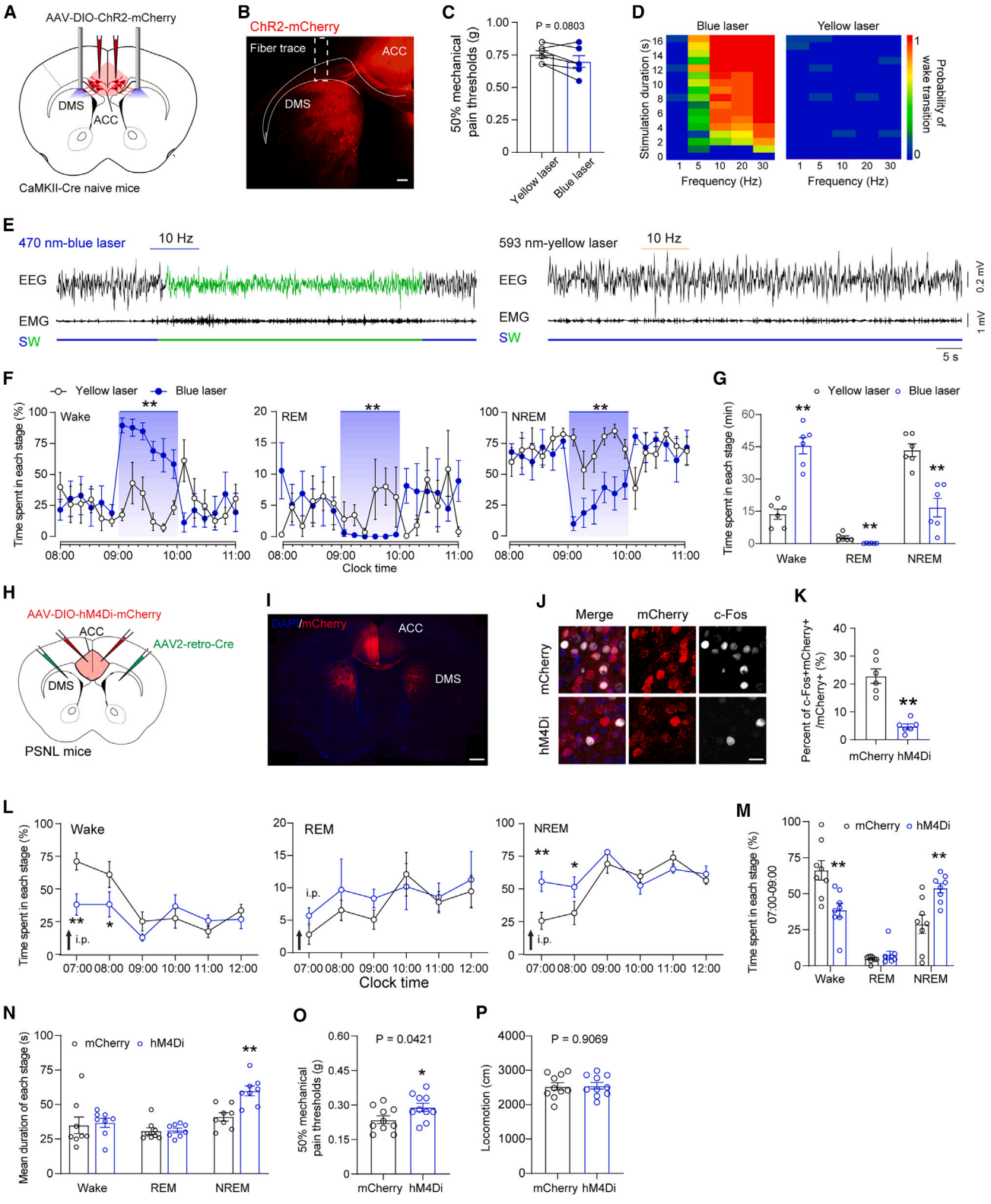

Figure 4. Hyperactivity of the ACC-DMS pathway induced sleep loss

(A) Diagram of optogenetic stimulation of ACC-DMS pathway *in vivo*. AAV-DIO-ChR2-mCherry was bilaterally injected into the ACC, with bilateral optic fibers implanted above the DMS.

(legend continued on next page)

Please cite this article in press as: Li et al., Anterior cingulate cortex projections to the dorsal medial striatum underlie insomnia associated with chronic pain, Neuron (2024), https://doi.org/10.1016/j.neuron.2024.01.014

identify D2R-MSNs, whereas DMS cells lacking GFP but exhibiting typical morphology and electrophysiological characteristics of MSNs were identified as D1R-MSNs (Figure 5A). Compared with the sham mice, the intrinsic excitability of D1R-MSNs, but not D2R-MSNs, was distinctly increased in PSNL mice (Figures 5B–5D). To assess the membrane excitability of D1R-MSNs in the PSNL mice, the spontaneous EPSCs (sEPSCs) and mEPSCs of postsynaptic AMPARs were analyzed. Notably, the amplitude of sEPSCs and mEPSCs was simultaneously increased in the D1R-MSNs of PSNL mice (Figures 5E, 5F, 5H, and 5I), indicating an increase in the numbers or functions of postsynaptic AMPARs of D1R-MSNs. More importantly, the frequency of sEPSCs and mEPSCs was also increased in D1R-MSNs in PSNL mice, indicating that chronic pain enhances the release of presynaptic glutamate to D1R-MSNs (Figures 5G and 5J). By contrast, neither frequency nor amplitude of sEPSCs and mEPSCs was changed in D2R-MSNs after PSNL (Figures S5G–S5L). These results suggest that chronic pain significantly increases the presynaptic excitatory inputs to DMS D1R-MSNs and changed postsynaptic AMPARs in PSNL mice.

Increased synaptic plasticity of ACC-DMS D1R-MSNs in chronic pain

Next, we tested whether PSNL-increased presynaptic glutamate inputs to DMS D1R-MSNs are from ACC PNs. We first investigated the long-term potentiation (LTP) in ACC PNs to DMS MSNs' synapses to determine whether chronic pain would contribute to the changes in corticostriatal synaptic plasticity in PSNL mice. High-frequency stimulation was applied in the ACC using an electrode to trigger LTP in DMS MSNs in acute slices from D2R-EGFP mice, 7–14 days after sham/PSNL administration (Figures 6A and 6B). In PSNL mice, AMPAR-dependent LTP increased in DMS D1R-MSNs but reduced in D2R-MSNs (Figures 6C and 6D), indicating increased plasticity of ACC PNs-DMS D1R-MSNs. Simultaneously, the increased LTP in D1R-MSNs was associated with a reduction in the paired-pulse ratio (PPR) (Figure 6E), indicating that the presynaptic ACC glutamate release probability was increased in PSNL mice. In contrast, the increased PPR of D2R-MSNs may be responsible for the decreased LTP in PSNL mice (Figure 6F).

In addition to the adaptation of AMPARs and presynaptic neurotransmitters, NMDARs are also important elements in pain signaling.[27,28] Thus, we checked the ratio of NMDAR-mediated excitatory currents to AMPAR-mediated EPSCs (NMDAR/AMPAR ratio) by using optogenetic approaches to examine the specific glutamatergic afferents of ACC PNs to DMS MSNs. AAV-based tracing confirmed the morphological associations of ACC PNs and DMS D1R-/D2R-MSNs (Figures 6G and 6H). We, therefore, injected AAV-CaMKII-ChR2-mCherry into the ACC and stimulated ACC-DMS terminals with blue light to induce NMDAR/AMPAR currents. As a result, the NMDAR/AMPAR ratio was significantly higher in D1R-MSNs from PSNL mice but was not changed in D2R-MSNs (Figures 6I and 6J), suggesting that chronic pain increased NMDAR-mediated synaptic transmission in D1R-MSNs. These results thus far suggested that the adaptation of AMPARs, presynaptic neurotransmitters, and NMDARs provide a molecular basis for the changes in corticostriatal synaptic plasticity in chronic pain.

Furthermore, we evaluated whether synaptic plasticity occurred at the onset of neuropathic pain in PSNL mice. Slices were prepared from animals 3–4 days after PSNL, and AMPAR-dependent LTP and PPR were measured in these mice. In contrast to the changes found 7–14 days after PSNL, none of these measures were changed in the early phase (3–4 days) of the neuropathic pain onset (Figures S7A–S7H). Together, these results indicate that chronic pain progressively induced significant synaptic plasticity of ACC-DMS D1R-MSNs synapse.

DMS D1R-MSNs mediate chronic-pain-induced insomnia

To determine whether activation of DMS D1R-MSNs is necessary for chronic-pain-induced insomnia, we injected AAV-DIO-hM4Di-mCherry into the DMS to silence D1R-MSNs selectively (Figures 7A and 7B). The inhibitory effect was validated by slice electrophysiological recordings (Figure 7C). Interestingly, we observed only a trend toward increased mechanical thresholds

(B) A representative image showing ACC PNs to DMS projections. Scale bars, 100 μm.
(C) Mechanical pain thresholds after optogenetic activation of ACC-DMS projections in naive mice. n = 6 mice, paired t test.
(D) Heatmap showing the mean probability of NREM sleep-to-wake transitions in relation to frequency and latency of stimulation induced by blue light (left) or yellow light (right).
(E) Representative EEG and EMG traces showing that blue light (left), but not yellow light (right), stimulation (16 s, 10 Hz) applied into the DMS during NREM sleep induced a rapid transition to wakefulness.
(F) Time course of wakefulness, REM sleep, and NREM sleep before, during, and after 1-h light stimulation. 10 Hz, 10 s ON/20 s OFF blue light stimulation (yellow light as control) was applied in the DMS during 09:00–10:00. n = 6 mice, using repeated-measures ANOVA, followed by Tukey post hoc test.
(G) Total time spent in each stage during laser stimulation in (F). n = 6 mice, using paired t test.
(H) Schematic diagram of chemogenetic inhibition of DMS-projecting ACC neurons. AAV2-retro-Cre was bilaterally injected into the DMS and AAV-hSyn-DIO-hM4Di-mCherry was bilaterally injected into the ACC in PSNL mice.
(I) A representative image showing Cre-dependent expression of hM4Di-mCherry in the ACC and the projections to the DMS. Scale bars, 500 μm.
(J and K) Representative images (J) and quantification (K) of c-Fos expression in ACC PNs 90 min after CNO administration in PSNL mice transduced with mCherry or hM4Di-mCherry in the ACC. Scale bars, 20 μm. n = 6 mice for each group, unpaired t test.
(L) Time course changes in wake, REM, and NREM sleep after chemogenetic inhibition of DMS-projecting ACC neurons in PSNL mice. n = 8 mice for each group, repeated-measures ANOVA, followed by Tukey post hoc test.
(M) Total time spent in each stage in 2 h after CNO administration (07:00–09:00) in (L). n = 8 mice for each group, using unpaired t test.
(N) Mean duration of each stage in 2 h after CNO administration (07:00–09:00) in (L). n = 8 mice for each group, using unpaired t test.
(O) Mechanical pain thresholds after inhibition of ACC PNs in PSNL mice. n = 10 mice for each group, unpaired t test.
(P) Locomotion in the open-field test after chemogenetic inhibition of DMS-projecting ACC PNs. n = 10 mice for each group, unpaired t test.
Data are shown as mean ± SEM. *$p < 0.05$, **$p < 0.01$. See also Figures S4–S6.

Please cite this article in press as: Li et al., Anterior cingulate cortex projections to the dorsal medial striatum underlie insomnia associated with chronic pain, Neuron (2024), https://doi.org/10.1016/j.neuron.2024.01.014

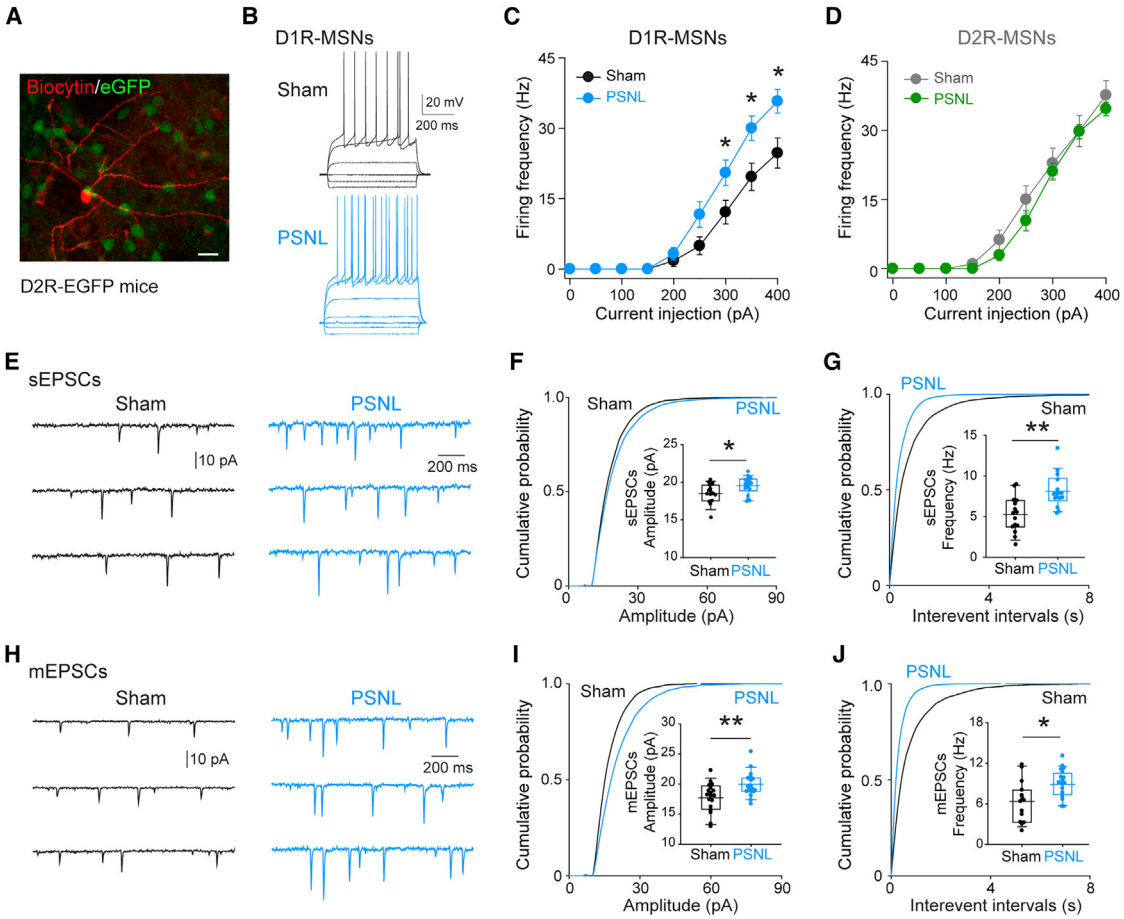

Figure 5. PSNL increased DMS D1R-MSNs synaptic excitability

(A) A representative image of DMS in D2R-EGFP mice. D2R-MSNs were identified by EGFP (green), while D1R-MSNs were identified by typical morphology of MSNs (biocytin injected, red) and did not overlap with GFP. Scale bars, 20 μm.

(B) Representative voltage traces showing responses of DMS D1R-MSNs to injections of depolarizing currents.

(C) Membrane excitability of DMS D1R-MSNs was increased in PSNL mice. n = 16 neurons from 5 sham mice, n = 18 neurons from 5 PSNL mice. *p < 0.05, by repeated-measures ANOVA.

(D) Membrane excitability of DMS D2R-MSNs was not changed in PSNL mice. n = 16 neurons from 5 sham mice, n = 18 neurons from 5 PSNL mice.

(E) Sample traces of sEPSCs recorded from DMS D1R-MSNs of sham and PSNL mice.

(F and G) Quantification of amplitude (F) and frequency (G) of sEPSCs of D1R-MSNs. n = 17 neurons from 5 mice per group.

(H) Sample traces of mEPSCs recorded from DMS D1R-MSNs of sham and PSNL mice.

(I and J) Quantification of amplitude (I) and frequency (J) of mEPSCs of D1R-MSNs. n = 16 neurons from 6 sham mice, n = 20 neurons from 6 PSNL mice.

Data are shown as mean ± SEM. *p < 0.05, **p < 0.01 by unpaired t test. See also Figure S5.

in PSNL mice when inhibiting DMS D1R-MSNs, without a statistical significance (Figure 7D). Importantly, chemogenetic inhibition of D1R-MSNs in the DMS decreased wakefulness for 2 h after CNO administration (07:00–09:00), concomitant with an increase in NREM sleep in PSNL, but not naive, mice as compared with vehicle controls (Figures 7E and 7F). These results indicate that inhibition of DMS D1R-MSNs partially blocked chronic-pain-induced insomnia.

DISCUSSION

More than half of patients with chronic pain complain of sleep loss, but neural circuits underlying chronic-pain-induced sleep disorders are poorly understood. In this study, we revealed that the hyperactivity of ACC PNs plays a key role in chronic-pain-induced insomnia through DMS projections (Figure S7I). Hyperactivity of ACC PNs occurred selectively during periods of chronic-pain-induced insomnia, as demonstrated by *in vivo* calcium imaging. Furthermore, cell-type-selective ablation of ACC PNs in PSNL mice and chemogenetic activation of ACC PNs in the naive mice demonstrated that hyperactivity of ACC PNs is sufficient and necessary for chronic-pain-induced insomnia. Importantly, we dissected the ACC PNs to DMS pathway in regulating chronic-pain-induced insomnia and found enhanced plasticity of ACC-DMS D1R-MSNs in PSNL mice. We further demonstrated that inhibition of DMS D1R-MSNs alleviates chronic-pain-induced insomnia. Our findings address a long-standing gap in the understanding

Please cite this article in press as: Li et al., Anterior cingulate cortex projections to the dorsal medial striatum underlie insomnia associated with chronic pain, Neuron (2024), https://doi.org/10.1016/j.neuron.2024.01.014

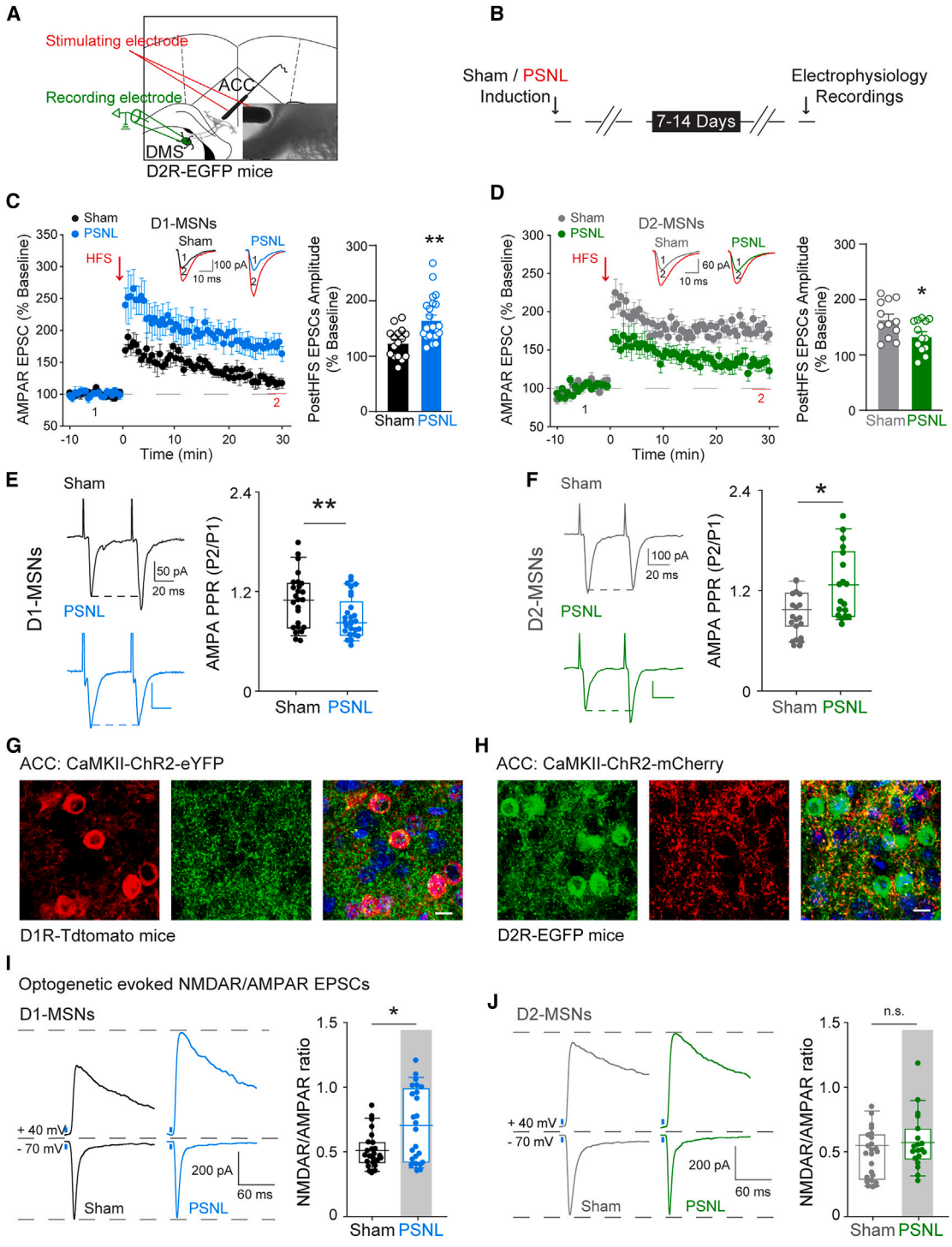

Figure 6. Enhanced synaptic plasticity of ACC-DMS D1R-MSNs synapses in PSNL mice

(A) Composite image of a vertical slice and vertical diagram of D2R-EGFP mouse brain. A stimulating electrode was placed in the ACC and D1R-MSNs/D2R-MSNs in the DMS were recorded.

(B) Schematic of the experiment. Slice recording was performed 7–14 days after PSNL.

(C) Facilitated LTP induction in DMS D1R-MSNs in PSNL mice. Left: time course of EPSC amplitude plotted as percent of baseline (0–10 min). Inserts: raw traces show examples of EPSCs evoked before (1) and 30 min after (2) high-frequency stimulation (HFS) protocol. Right: quantification of EPSC amplitude (% baseline) after 20–30 min of HFS. n = 16 neurons from 10 sham mice, n = 25 neurons from 10 PSNL mice.

(legend continued on next page)

Please cite this article in press as: Li et al., Anterior cingulate cortex projections to the dorsal medial striatum underlie insomnia associated with chronic pain, Neuron (2024), https://doi.org/10.1016/j.neuron.2024.01.014

of how chronic pain induces sleep disorders by showing that ACC PN hyperactivity selectively controls chronic-pain-induced insomnia via reshaping the plasticity of ACC PNs to DMS D1R-MSNs synapses.

Our study identifies a central cortical region that specifically controls chronic-pain-induced insomnia. First, activity of ACC PNs was specifically increased in chronic-pain-induced insomnia, while reducing pain sensitivity or increasing sleep alone could not reverse the hyperactivity of ACC PNs during insomnia in PSNL mice. Second, when ACC PNs were ablated, chronic-pain-induced insomnia was completely blocked, while the mechanical pain thresholds remained lower than those of mice without chronic pain. Third, activation of ACC PNs in naive mice induced sleep loss but did not decrease mechanical pain thresholds. These results highlight the crucial involvement of ACC PNs in insomnia specifically associated with chronic pain. Notably, analgesics such as morphine and gabapentin exhibit intricate mechanisms in influencing the activity of ACC PNs, potentially extending beyond the realm of insomnia induced by chronic pain. It will be interesting to test the activity of ACC PNs during treatment with peripheral analgesics in future studies. The ACC is known to be one of the most consistently activated brain regions in response to chronic pain, and it also regulates pain sensitivity and affective behaviors,[29,30] receiving numerous excitatory afferents from cortical areas, the basal forebrain, thalamus, hypothalamus, and the monoaminergic centers in the brainstem.[31] This intricate network may contribute to the overactivation of ACC PNs in a chronic pain state.

The ACC sends the densest output to the DMS, which modulates action,[32] motivation, and decision-making.[33] DMS D1R-MSNs and D2R-MSNs are innervated by ACC PNs, but our results showed that hyperactivity of ACC PNs in chronic pain selectively increases excitatory connections with DMS D1R-MSNs, resulting in increased sEPSCs and mEPSCs, LTP, and the NMDAR/AMPAR ratio and decreased PPR in DMS D1R-MSNs, while D2R-MSNs were lacking these changes. Interestingly, the NAc in the ventral striatum also receives glutamatergic ACC inputs and controls the social transfer of pain.[26] Lower mEPSCs, with a reduced AMPAR/NMDAR ratio from cortical stimulation, are found specifically in NAc D2R-MSNs in neuropathic pain model mice.[34] Moreover, decreased excitatory synaptic transmission in NAc D2R-MSNs is required for decreased motivation during chronic pain.[35] These findings indicate that the ACC-NAc pathway may be more central to the regulation of emotional aspects, whereas the ACC-DMS pathway appears to be selectively involved in insomnia in the context of chronic pain.

Our finding that chemogenetic inhibition of DMS D1R-MSNs did not completely block chronic-pain-induced insomnia could be due to incomplete manipulation of the DMS D1R-MSN population or diffuse network effects. In recent decades, several wake-promoting brain regions were found to be directly activated during chronic pain, such as the locus coeruleus,[36–38] dorsal raphe,[4,39] and parabrachial nuclei (PB).[40] For example, activation of glutamatergic lateral PB neurons induces neuropathic pain-like behavior[41–43] and promotes wakefulness.[44–46] However, it remains uncertain whether neurons in these brain regions activated by chronic pain also specifically regulate insomnia. Furthermore, chronic pain mice do not exhibit heightened wakefulness during the dark phase, mirroring the behavior of chronic pain patients who do not display increased activity during the daytime. This implies that chronic-pain-induced insomnia may not be directly regulated by these physiologically powerful wake-promoting neurons. Therefore, further investigation is needed to determine whether these wake-promoting neurons specifically become activated in chronic pain. It is also important to explore whether the loss of function in these regions can fully block insomnia without affecting pain sensitivity.

In chronic pain conditions, two distinct types of ACC neurons—GABAergic neurons and glutamatergic neurons—are both activated but play different roles in pain processing. ACC GABAergic neurons primarily regulate nociceptive hypersensitivity in conditions of low cortical activity.[24] Furthermore, sleep disturbances in a neuropathic-pain-like condition in the mouse are associated with altered GABAergic transmission in the cingulate cortex.[47] The interactions and local connections between these two types of neurons are likely more complex than simple direct activation or inhibition. Notably, certain GABAergic neurons can inhibit other GABAergic interneurons, leading to disinhibition of glutamatergic neurons.[48] This intricate balance between ACC GABAergic and glutamatergic neurons is crucial for normal physiological functioning. However, disruptions to this delicate balance can potentially result in allodynia, accompanied by symptoms such as insomnia and depression. Understanding these complex interactions between ACC GABAergic and glutamatergic neurons is vital for unraveling the mechanisms underlying chronic-pain-related symptoms.[49]

(D) Reduced LTP induction in DMS D2R-MSNs in PSNL mice. Left: time course of EPSC amplitude plotted as percent of baseline (0–10 min). Inserts: raw traces show examples of EPSCs evoked before (1) and 30 min after (2) HFS protocol. Right: quantification of EPSC amplitude (% baseline) after 20–30 min of HFS. n = 12 neurons from 9 sham mice, n = 13 neurons from 9 PSNL mice.

(E and F) Left: sample traces showing PPR (50-ms interstimulus interval) measured in D1R-MSNs (E) or D2R-MSNs (F) from sham and PSNL mice. Right: averaged data showing a decreased PPR in D1R-MSNs (E), but an increased PPR in D2R-MSNs (F), after PSNL induction. D1R-MSNs: n = 25 neurons from 10 sham mice, n = 29 neurons from 10 PSNL mice; D2R-MSNs: n = 20 neurons from 9 sham mice, n = 18 neurons from 9 PSNL mice.

(G) Terminal of eYFP+ ACC PNs was closely associated with DMS D1R-MSNs of D1R-tdTomato mice. Scale bars, 10 μm.

(H) Terminal of mCherry+ ACC PNs was closely associated with DMS D2R-MSNs of D2R-eGFP mice. Scale bars, 10 μm.

(I and J) Left: sample traces of NMDAR-EPSCs were recorded at +40 mV (top traces), and AMPAR-EPSCs were recorded at −70 mV (bottom traces) from DMS D1R-MSNs (I) and D2R-MSNs (J) in sham and PSNL mice. AMPAR-EPSC amplitudes were normalized to peaks at −70 mV. Right: quantification of NMDAR/AMPAR currents ratio in D1R-MSNs and D2R-MSNs. D1R-MSNs: n = 22 neurons from 4 mice per group; D2R-MSNs: n = 20 neurons from 4 mice per group. Data are shown as mean ± SEM. *p < 0.05, **p < 0.01, using unpaired t test. See also Figure S7.

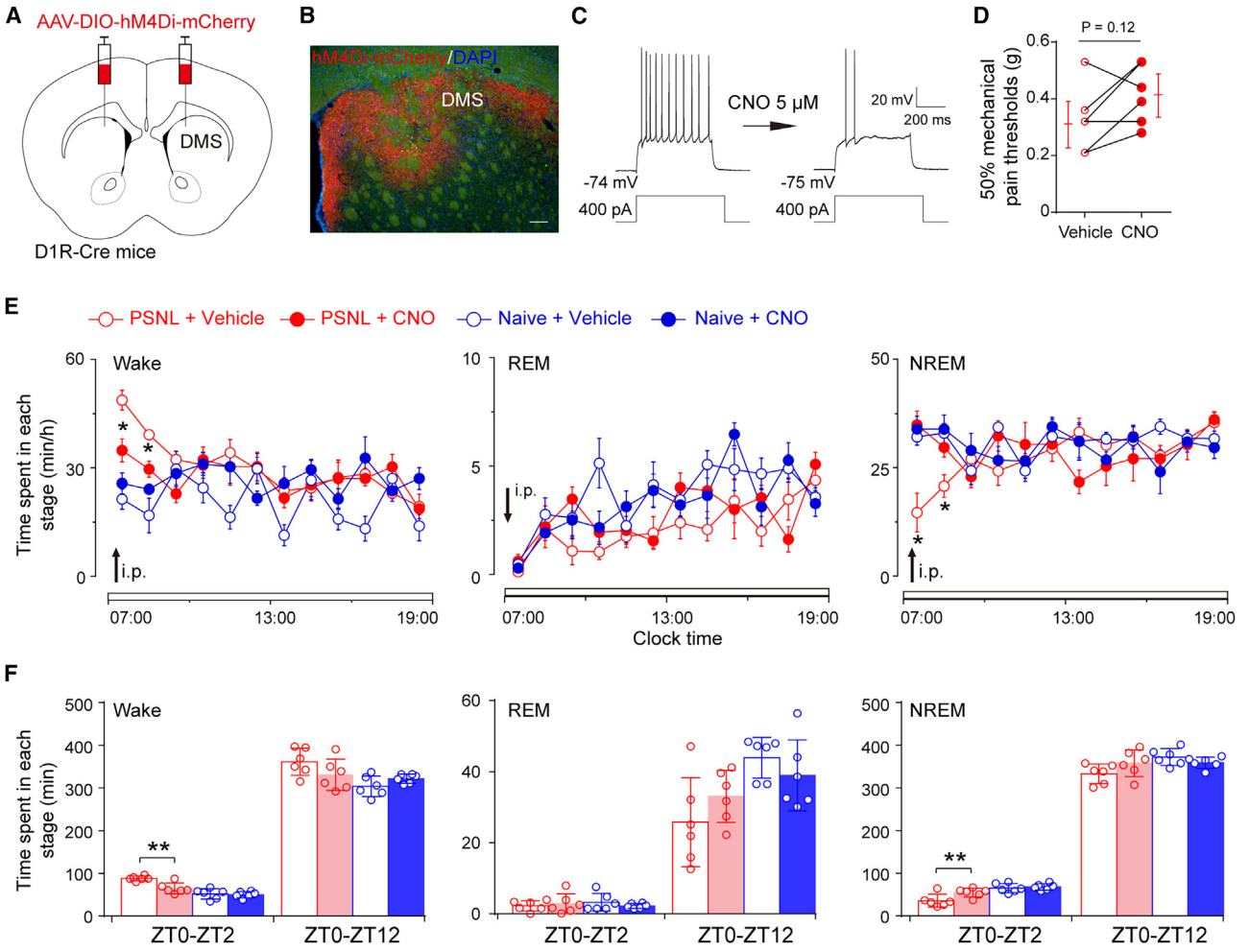

Figure 7. Inhibition of DMS D1R-MSNs attenuated insomnia in PSNL mice

(A) Schematic diagram of chemogenetic inhibition of DMS D1R-MSNs. Two injections of AAV-DIO-hM4Di-mCherry on each hemisphere were injected into the DMS in D1R-Cre mice.

(B) A representative image showing hM4Di-mCherry expression in the DMS. Scale bars, 200 μm.

(C) Representative electrophysiological traces showing chemogenetic inhibition of DMS D1R-MSNs.

(D) Mechanical pain thresholds in D1R-Cre PSNL mice after CNO injection. n = 6 mice, paired t test.

(E) Time course of time spent in each stage after CNO administration at 06:50. n = 6 mice, using repeated-measures ANOVA, followed by Tukey post hoc test.

(F) Total time spent in each stage from 07:00 to 09:00 and 07:00 to 19:00 after CNO administration at 06:50 in (E). n = 6 mice for each group, using two-way ANOVA, followed by Tukey post hoc test.

Data are shown as mean ± SEM. *p < 0.05, **p < 0.01.

In summary, our study provides valuable insights into chronic-pain-induced insomnia and highlights the specific involvement of ACC PNs and the ACC-DMS D1R-MSNs' synapse plasticity.

STAR★METHODS

Detailed methods are provided in the online version of this paper and include the following:

SUPPLEMENTAL INFORMATION

Supplemental information can be found online at https://doi.org/10.1016/j.neuron.2024.01.014.

ACKNOWLEDGMENTS

This study was supported by the STI2030-Major Project (2021ZD0203400 to Z.-L.H.); the National Natural Science Foundation of China (32371028 to Y.-D.L., 32300822 to Y.-J.L., 82020108014 and 32070984 to Z.-L.H., and 82071491 and 31871072 to W.-M.Q.); the Shanghai Municipal Science and Technology Major Project (2018SHZDZX01 to Z.-L.H.); the ZJLab Program for Shanghai Outstanding Academic Leaders (to Z.-L.H.); the Shanghai Center for Brain Science and Brain-Inspired Technology and Lingang Laboratory & National Key Laboratory of Human Factors Engineering Joint Grant (LG-TKN-202203-01 to Z.-L.H.); Shanghai Municipal Health Commission (202340046 to Y.-D.L.); and the Shanghai Jiao Tong University 2030 Initiative (to Y.-D.L.). M.L. was supported by the Japan Society for the Promotion of Science (JP21H02802 and JP22K21351); the Japan Agency for Medical Research and Development (AMED) Moonshot Programme (JP21zf0127005); and the World Premier International Research Center Initiative (WPI) of the Ministry of Education, Culture, Sports, Science and Technology (MEXT).

AUTHOR CONTRIBUTIONS

Y.-D.L., Z.-L.L., and Z.-L.H. designed the experiments; Z.-L.H. and W.-M.Q. provided mentorship of the project; Y.-D.L., Y.-J.L., W.-K.S., and Z.-K.C. performed the *in vivo* experiments; J.G., Y.-J.L., and Z.-L.L. collected and analyzed electrophysiological data; L.W. helped with electrophysiological analysis; Y.-D.L., Y.-J.L., and Z.-L.H. wrote the manuscript with assistance from Z.-L.L., W.-M.Q., W.-K.S., M.L., and A.C.; and all of the authors discussed the manuscript.

DECLARATION OF INTERESTS

The authors declare no competing interests.

Received: August 26, 2023
Revised: November 29, 2023
Accepted: January 12, 2024
Published: February 13, 2024

REFERENCES

1. Elliott, A.M., Smith, B.H., Penny, K.I., Smith, W.C., and Chambers, W.A. (1999). The epidemiology of chronic pain in the community. Lancet *354*, 1248–1252.
2. Simon, G.E., VonKorff, M., Piccinelli, M., Fullerton, C., and Ormel, J. (1999). An international study of the relation between somatic symptoms and depression. N. Engl. J. Med. *341*, 1329–1335.
3. McWilliams, L.A., Goodwin, R.D., and Cox, B.J. (2004). Depression and anxiety associated with three pain conditions: results from a nationally representative sample. Pain *111*, 77–83.
4. Zhou, W., Jin, Y., Meng, Q., Zhu, X., Bai, T., Tian, Y., Mao, Y., Wang, L., Xie, W., Zhong, H., et al. (2019). A neural circuit for comorbid depressive symptoms in chronic pain. Nat. Neurosci. *22*, 1649–1658.
5. Bushnell, M.C., Ceko, M., and Low, L.A. (2013). Cognitive and emotional control of pain and its disruption in chronic pain. Nat. Rev. Neurosci. *14*, 502–511.
6. Sandkühler, J. (2000). Learning and memory in pain pathways. Pain *88*, 113–118.
7. Haack, M., Simpson, N., Sethna, N., Kaur, S., and Mullington, J. (2020). Sleep deficiency and chronic pain: potential underlying mechanisms and clinical implications. Neuropsychopharmacology *45*, 205–216.
8. Cheatle, M.D., Foster, S., Pinkett, A., Lesneski, M., Qu, D., and Dhingra, L. (2016). Assessing and Managing Sleep Disturbance in Patients with Chronic Pain. Anesthesiol. Clin. *34*, 379–393.
9. Finan, P.H., Goodin, B.R., and Smith, M.T. (2013). The association of sleep and pain: an update and a path forward. J. Pain *14*, 1539–1552.
10. Aasvik, J., Stiles, T.C., Woodhouse, A., Borchgrevink, P., and Inge Landrø, N. (2018). The Effect of Insomnia on Neuropsychological Functioning in Patients with Comorbid Symptoms of Pain, Fatigue, and Mood Disorders. Arch. Clin. Neuropsychol. *33*, 14–23.
11. Curtis, A.F., Williams, J.M., McCoy, K.J.M., and McCrae, C.S. (2018). Chronic Pain, Sleep, and Cognition in Older Adults With Insomnia: A Daily Multilevel Analysis. J. Clin. Sleep Med. *14*, 1765–1772.
12. Finan, P.H., and Smith, M.T. (2013). The comorbidity of insomnia, chronic pain, and depression: dopamine as a putative mechanism. Sleep Med. Rev. *17*, 173–183.
13. Lazarus, M., Huang, Z.L., Lu, J., Urade, Y., and Chen, J.F. (2012). How do the basal ganglia regulate sleep-wake behavior? Trends Neurosci. *35*, 723–732.
14. Dong, H., Chen, Z.K., Guo, H., Yuan, X.S., Liu, C.W., Qu, W.M., and Huang, Z.L. (2022). Striatal neurons expressing dopamine D1 receptor promote wakefulness in mice. Curr. Biol. *32*, 600–613.e4.
15. Yuan, X.S., Wang, L., Dong, H., Qu, W.M., Yang, S.R., Cherasse, Y., Lazarus, M., Schiffmann, S.N., D'Exaerde, A.K., Li, R.X., et al. (2017). Striatal adenosine A2A receptor neurons control active-period sleep via parvalbumin neurons in external globus pallidus. eLife *6*, e29055.
16. Zhao, R., Zhou, H., Huang, L., Xie, Z., Wang, J., Gan, W.B., and Yang, G. (2018). Neuropathic Pain Causes Pyramidal Neuronal Hyperactivity in the Anterior Cingulate Cortex. Front. Cell. Neurosci. *12*, 107.
17. Li, X.Y., Ko, H.G., Chen, T., Descalzi, G., Koga, K., Wang, H., Kim, S.S., Shang, Y., Kwak, C., Park, S.W., et al. (2010). Alleviating neuropathic pain hypersensitivity by inhibiting PKMzeta in the anterior cingulate cortex. Science *330*, 1400–1404.
18. Bliss, T.V., Collingridge, G.L., Kaang, B.K., and Zhuo, M. (2016). Synaptic plasticity in the anterior cingulate cortex in acute and chronic pain. Nat. Rev. Neurosci. *17*, 485–496.
19. Chiou, C.S., Chen, C.C., Tsai, T.C., Huang, C.C., Chou, D., and Hsu, K.S. (2016). Alleviating Bone Cancer-induced Mechanical Hypersensitivity by Inhibiting Neuronal Activity in the Anterior Cingulate Cortex. Anesthesiology *125*, 779–792.
20. Chen, T., Taniguchi, W., Chen, Q.Y., Tozaki-Saitoh, H., Song, Q., Liu, R.H., Koga, K., Matsuda, T., Kaito-Sugimura, Y., Wang, J., et al. (2018). Top-down descending facilitation of spinal sensory excitatory transmission from the anterior cingulate cortex. Nat. Commun. *9*, 1886.
21. Gompf, H.S., Mathai, C., Fuller, P.M., Wood, D.A., Pedersen, N.P., Saper, C.B., and Lu, J. (2010). Locus ceruleus and anterior cingulate cortex sustain wakefulness in a novel environment. J. Neurosci. *30*, 14543–14551.
22. Wu, Z., Fang, X., Yu, L., Wang, D., Liu, R., Teng, X., Guo, C., Ren, J., and Zhang, C. (2022). Abnormal functional connectivity of the anterior cingulate cortex subregions mediates the association between anhedonia and sleep quality in major depressive disorder. J. Affect. Disord. *296*, 400–407.
23. Wu, Y.E., Li, Y.D., Luo, Y.J., Wang, T.X., Wang, H.J., Chen, S.N., Qu, W.M., and Huang, Z.L. (2015). Gelsemine alleviates both neuropathic pain and sleep disturbance in partial sciatic nerve ligation mice. Acta Pharmacol. Sin. *36*, 1308–1317.
24. Li, Y.D., Ge, J., Luo, Y.J., Xu, W., Wang, J., Lazarus, M., Hong, Z.Y., Qu, W.M., and Huang, Z.L. (2020). High cortical delta power correlates with aggravated allodynia by activating anterior cingulate cortex GABAergic neurons in neuropathic pain mice. Pain *161*, 288–299.
25. Liu, Y.Y., Yin, D., Chen, L., Qu, W.M., Chen, C.R., Laudon, M., Cheng, N.N., Urade, Y., and Huang, Z.L. (2014). Piromelatine exerts

antinociceptive effect via melatonin, opioid, and 5HT1A receptors and hypnotic effect via melatonin receptors in a mouse model of neuropathic pain. Psychopharmacol. (Berl.) *231*, 3973–3985.

26. Smith, M.L., Asada, N., and Malenka, R.C. (2021). Anterior cingulate inputs to nucleus accumbens control the social transfer of pain and analgesia. Science *371*, 153–159.
27. Li, X.H., Miao, H.H., and Zhuo, M. (2019). NMDA Receptor Dependent Long-term Potentiation in Chronic Pain. Neurochem. Res. *44*, 531–538.
28. Zhuo, M. (2009). Plasticity of NMDA receptor NR2B subunit in memory and chronic pain. Mol. Brain *2*, 4.
29. Barthas, F., Sellmeijer, J., Hugel, S., Waltisperger, E., Barrot, M., and Yalcin, I. (2015). The anterior cingulate cortex is a critical hub for pain-induced depression. Biol. Psychiatry *77*, 236–245.
30. Zhuo, M. (2007). A synaptic model for pain: long-term potentiation in the anterior cingulate cortex. Mol. Cells *23*, 259–271.
31. Fillinger, C., Yalcin, I., Barrot, M., and Veinante, P. (2017). Afferents to anterior cingulate areas 24a and 24b and midcingulate areas 24a' and 24b′ in the mouse. Brain Struct. Funct. *222*, 1509–1532.
32. Brockett, A.T., Tennyson, S.S., deBettencourt, C.A., Gaye, F., and Roesch, M.R. (2020). Anterior cingulate cortex is necessary for adaptation of action plans. Proc. Natl. Acad. Sci. USA *117*, 6196–6204.
33. Cox, J., Minerva, A.R., Fleming, W.T., Zimmerman, C.A., Hayes, C., Zorowitz, S., Bandi, A., Ornelas, S., McMannon, B., Parker, N.F., et al. (2023). A neural substrate of sex-dependent modulation of motivation. Nat. Neurosci. *26*, 274–284.
34. Ren, W., Centeno, M.V., Berger, S., Wu, Y., Na, X., Liu, X., Kondapalli, J., Apkarian, A.V., Martina, M., and Surmeier, D.J. (2016). The indirect pathway of the nucleus accumbens shell amplifies neuropathic pain. Nat. Neurosci. *19*, 220–222.
35. Schwartz, N., Temkin, P., Jurado, S., Lim, B.K., Heifets, B.D., Polepalli, J.S., and Malenka, R.C. (2014). Chronic pain. Decreased motivation during chronic pain requires long-term depression in the nucleus accumbens. Science *345*, 535–542.
36. Alba-Delgado, C., Llorca-Torralba, M., Horrillo, I., Ortega, J.E., Mico, J.A., Sánchez-Blázquez, P., Meana, J.J., and Berrocoso, E. (2013). Chronic pain leads to concomitant noradrenergic impairment and mood disorders. Biol. Psychiatry *73*, 54–62.
37. Suárez-Pereira, I., Llorca-Torralba, M., Bravo, L., Camarena-Delgado, C., Soriano-Mas, C., and Berrocoso, E. (2022). The Role of the Locus Coeruleus in Pain and Associated Stress-Related Disorders. Biol. Psychiatry *91*, 786–797.
38. Kohro, Y., Matsuda, T., Yoshihara, K., Kohno, K., Koga, K., Katsuragi, R., Oka, T., Tashima, R., Muneta, S., Yamane, T., et al. (2020). Spinal astrocytes in superficial laminae gate brainstem descending control of mechanosensory hypersensitivity. Nat. Neurosci. *23*, 1376–1387.
39. Yu, W., Pati, D., Pina, M.M., Schmidt, K.T., Boyt, K.M., Hunker, A.C., Zweifel, L.S., McElligott, Z.A., and Kash, T.L. (2021). Periaqueductal gray/dorsal raphe dopamine neurons contribute to sex differences in pain-related behaviors. Neuron *109*, 1365–1380.e5.
40. Choi, S., Hachisuka, J., Brett, M.A., Magee, A.R., Omori, Y., Iqbal, N.U., Zhang, D., DeLisle, M.M., Wolfson, R.L., Bai, L., et al. (2020). Parallel ascending spinal pathways for affective touch and pain. Nature *587*, 258–263.
41. Sun, L., Liu, R., Guo, F., Wen, M.Q., Ma, X.L., Li, K.Y., Sun, H., Xu, C.L., Li, Y.Y., Wu, M.Y., et al. (2020). Parabrachial nucleus circuit governs neuropathic pain-like behavior. Nat. Commun. *11*, 5974.
42. Deng, J., Zhou, H., Lin, J.K., Shen, Z.X., Chen, W.Z., Wang, L.H., Li, Q., Mu, D., Wei, Y.C., Xu, X.H., et al. (2020). The Parabrachial Nucleus Directly Channels Spinal Nociceptive Signals to the Intralaminar Thalamic Nuclei, but Not the Amygdala. Neuron *107*, 909–923.e6.
43. Yang, H., de Jong, J.W., Cerniauskas, I., Peck, J.R., Lim, B.K., Gong, H., Fields, H.L., and Lammel, S. (2021). Pain modulates dopamine neurons via a spinal-parabrachial-mesencephalic circuit. Nat. Neurosci. *24*, 1402–1413.
44. Qiu, M.H., Chen, M.C., Fuller, P.M., and Lu, J. (2016). Stimulation of the Pontine Parabrachial Nucleus Promotes Wakefulness via Extra-thalamic Forebrain Circuit Nodes. Curr. Biol. *26*, 2301–2312.
45. Xu, Q., Wang, D.R., Dong, H., Chen, L., Lu, J., Lazarus, M., Cherasse, Y., Chen, G.H., Qu, W.M., and Huang, Z.L. (2021). Medial Parabrachial Nucleus Is Essential in Controlling Wakefulness in Rats. Front. Neurosci. *15*, 645877.
46. Bao, W.W., Jiang, S., Qu, W.M., Li, W.X., Miao, C.H., and Huang, Z.L. (2023). Understanding the Neural Mechanisms of General Anesthesia from Interaction with Sleep-Wake State: A Decade of Discovery. Pharmacol. Rev. *75*, 532–553.
47. Narita, M., Niikura, K., Nanjo-Niikura, K., Narita, M., Furuya, M., Yamashita, A., Saeki, M., Matsushima, Y., Imai, S., Shimizu, T., et al. (2011). Sleep disturbances in a neuropathic pain-like condition in the mouse are associated with altered GABAergic transmission in the cingulate cortex. Pain *152*, 1358–1372.
48. Apicella, A.J., and Marchionni, I. (2022). VIP-Expressing GABAergic Neurons: Disinhibitory vs. Inhibitory Motif and Its Role in Communication Across Neocortical Areas. Front. Cell. Neurosci. *16*, 811484.
49. Zhuo, M. (2008). Cortical excitation and chronic pain. Trends Neurosci. *31*, 199–207.
50. Li, Y.D., Luo, Y.J., Chen, Z.K., Quintanilla, L., Cherasse, Y., Zhang, L., Lazarus, M., Huang, Z.L., and Song, J. (2022). Hypothalamic modulation of adult hippocampal neurogenesis in mice confers activity-dependent regulation of memory and anxiety-like behavior. Nat. Neurosci. *25*, 630–645.
51. Luo, Y.J., Li, Y.D., Wang, L., Yang, S.R., Yuan, X.S., Wang, J., Cherasse, Y., Lazarus, M., Chen, J.F., Qu, W.M., et al. (2018). Nucleus accumbens controls wakefulness by a subpopulation of neurons expressing dopamine D1 receptors. Nat. Commun. *9*, 1576.
52. Qu, W.M., Xu, X.H., Yan, M.M., Wang, Y.Q., Urade, Y., and Huang, Z.L. (2010). Essential role of dopamine D2 receptor in the maintenance of wakefulness, but not in homeostatic regulation of sleep, in mice. J. Neurosci. *30*, 4382–4389.
53. Huang, Z.L., Qu, W.M., Eguchi, N., Chen, J.F., Schwarzschild, M.A., Fredholm, B.B., Urade, Y., and Hayaishi, O. (2005). Adenosine A2A, but not A1, receptors mediate the arousal effect of caffeine. Nat. Neurosci. *8*, 858–859.
54. Li, Y.D., Luo, Y.J., Xu, W., Ge, J., Cherasse, Y., Wang, Y.Q., Lazarus, M., Qu, W.M., and Huang, Z.L. (2021). Ventral pallidal GABAergic neurons control wakefulness associated with motivation through the ventral tegmental pathway. Mol. Psychiatry *26*, 2912–2928.
55. Li, Y., Bao, H., Luo, Y., Yoan, C., Sullivan, H.A., Quintanilla, L., Wickersham, I., Lazarus, M., Shih, Y.I., and Song, J. (2020). Supramammillary nucleus synchronizes with dentate gyrus to regulate spatial memory retrieval through glutamate release. eLife *9*, 1509–1532.
56. Li, Y.D., Luo, Y.J., Xie, L., Tart, D.S., Sheehy, R.N., Zhang, L., Coleman, L.G., Jr., Chen, X., and Song, J. (2023). Activation of hypothalamic-enhanced adult-born neurons restores cognitive and affective function in Alzheimer's disease. Cell Stem Cell *30*, 415–432.e6.
57. Luo, Y.J., Ge, J., Chen, Z.K., Liu, Z.L., Lazarus, M., Qu, W.M., Huang, Z.L., and Li, Y.D. (2023). Ventral pallidal glutamatergic neurons regulate wakefulness and emotion through separated projections. iScience *26*, 107385.

Please cite this article in press as: Li et al., Anterior cingulate cortex projections to the dorsal medial striatum underlie insomnia associated with chronic pain, Neuron (2024), https://doi.org/10.1016/j.neuron.2024.01.014

CellPress

STAR★METHODS

KEY RESOURCES TABLE

REAGENT or RESOURCE	SOURCE	IDENTIFIER
Antibodies		
Rabbit polyclonal anti-Fos	Millipore	Cat#ABE457; RRID: AB_2631318
Alexa Fluor 647 Donkey anti-Rabbit	Jackson ImmunoResearch	Cat#: 711-606-152; RRID: AB_2340625
Bacterial and virus strains		
AAV2/9-hSyn-DIO-hM3Dq-mCherry	Taitool Bioscience	Cat #S0192-9
AAV2/9-hSyn-DIO-hM4Di-mCherry	Taitool Bioscience	Cat #S0193-9
AAV9-hSyn-DIO-hChR2(H134R)-mCherry	Taitool Bioscience	Cat #S0165-9
AAV9-hSyn-CaMKII-hChR2(H134R)-eYFP	Brain VTA	Cat #PT0296
AAV9-hSyn-CaMKII-hChR2(H134R)-mCherry	Brain VTA	Cat #PT0296
AAV2/9-CAG-DIO-Caspase-3	Taitool Bioscience	Cat # S0236-1
AAV2/9-hSyn-DIO-eGFP	Taitool Bioscience	Cat # S0789-9
AAV2/9-hSyn-DIO-mCherry	Taitool Bioscience	Cat #S0240-9
AAV2/9-hSyn-FLEX-GCaMP6f	Taitool Bioscience	Cat #S0227-9
scAAV2/2-Retro-hSyn-Cre-pA	Taitool Bioscience	Cat #S0292-2R
Chemicals, peptides, and recombinant proteins		
NBQX	Tocris	Cat #0373
D-APV	Tocris	Cat #0106
biocytin	Sigma	Cat #B4261
Clozapine-N-oxide	LKT Laboratories	Cat #C4759
Diazepam	Tianjin Pharmaceutical Co., Ltd., China	N/A
Gabapentin	Chongqing Sai Wei Pharmaceutical Co. Ltd. , China	N/A
Morphine	Shenyang NO.1 Pharmaceutical Co., Ltd., China	N/A
Experimental models: Organisms/strains		
Mouse: CaMKII-Cre mice	Jackson laboratory	JAX stock #017535
Mouse: D1R-Cre mice B6.FVB(Cg)-Tg(Drd1a-Cre)	Mutant Mouse Resource Research Centers	Dr. Jiang-Fan Chen
D2R-eGFP mice	Jackson Laboratory (USA)	JAX stock #030537
D1R-tdTomato mice	Jackson Laboratory (USA)	JAX stock #016204
Software and algorithms		
SleepSign	Kissei Comtec	RRID: SCR_018200
Spike2 Software	Cambridge Electronic Design	RRID: SCR_000903
nVista 3	Inscopix	RRID:SCR_11286205
MATLAB R2014b	Mathworks	RRID:SCR_001622
Igor Pro	Wavemetrics	RRID: SCR_000325
FIJI	ImageJ	RRID: SCR_002285
pClamp 10.3	Molecular Devices	RRID: SCR_011323
Olympus FluoView	Olympus	RRID: SCR_014215
GraphPad Prism 8.0	Graphpad	RRID:SCR_002798
Adobe Illustrator	Adobe Systems	RRID: SCR_010279
Other		
microtome	Leica	Cat #CM1950
vibratome	Leica	Cat#VT1200
pipette puller	Narishige	Cat #PC-10

Please cite this article in press as: Li et al., Anterior cingulate cortex projections to the dorsal medial striatum underlie insomnia associated with chronic pain, Neuron (2024), https://doi.org/10.1016/j.neuron.2024.01.014

RESOURCE AVAILABILITY

Lead contact

Further information and requests for resources and reagents should be directed to and will be fulfilled by the Lead Contact, Ya-Dong Li (yadlee@126.com).

Materials availability

This study did not generate new unique reagents.

Data and code availability

- All data reported in this paper will be shared by the lead contact upon request.
- This paper does not report original code.
- Any additional information required to reanalyze the data reported in this paper is available from the lead contact upon request.

EXPERIMENTAL MODEL AND STUDY PARTICIPANT DETAILS

Experimental animals

Male and female mice with a body weight of 22–26 g (10–14 weeks old) were used in this study, but gender difference was not evaluated in this study. CaMKII-Cre mice (10–14 weeks old) were obtained from the Jackson Laboratory (Stock No: 017535). D1R-Cre (B6.FVB(Cg)-Tg(Drd1a-Cre) EY266Gsat/Mmucd, GENSAT) mice (10–14 weeks old) were kindly provided by Jiang-Fan Chen (Wenzhou Medical University). D1R-tdTomato mice (10–14 weeks old) were kindly provided by Ji Hu (ShanghaiTech University). D2R-EGFP mice (10–14 weeks old) were obtained from the Institute of Neuroscience, Chinese Academy of Science, Shanghai. The animals were maintained at room temperature (22 ± 0.5°C) and controlled humidity (60 ± 2%) under a 12-h light/12-h dark cycle (lights on at 07:00) and provided food and water *ad libitum*. No immune deficiencies or other health problems were observed in these lines, and all animals were experimentally and drug-naive before use. All experimental protocols were approved by the Medical Experimental Animal Administrative Committee of Fudan University.

METHOD DETAILS

EEG/EMG electrode-implantation surgery

Mice were anesthetized under 1.5−2.0% isoflurane in oxygen at a flow rate of 0.8 L/min and implanted with EEG and electromyogram (EMG) electrodes for polysomnographic recordings. Two stainless-steel screws were installed through the skull over the parietal and frontal cortices according to the brain atlas, which served as EEG electrodes. Two insulated, stainless-steel, Teflon-coated wire EMG electrodes were bilaterally inserted into the trapezius muscles. All the electrodes were gathered into a micro-connector and fixed to the skull with dental cement.

Virus injection and fiber implantation

Under anesthesia, mice were placed in a stereotaxic frame (RWD, Shenzhen, China). AAVs were injected by a fine glass electrode with a 15–20 μm tip containing virus was inserted bilaterally into the ACC (AP +0.7mm; ML ±0.3 mm; DV -1.8 mm) or DMS (AP +0.7/1.1 mm; ML ±1.25 mm; DV -2.5 mm). A total of 100 nL virus was delivered into each site over a 10-min period via nitrogen-gas pulses using an air-compression system. For AAV-DIO-hM4Di-mCherry injection, 2 injections in each striatum and 4 injections in total for each mouse. The needle was left in place for 10 min to permit diffusion. For optogenetic stimulation of ACC-DMS terminals, bilateral optic fibers (diameters = 200 um) were planted above the DMS (AP +0.7 mm; ML ±1.25 mm; DV -2.2 mm). Mice that received injections were used for experiments at least 2 weeks after viral injection.

EEG recordings and analysis

EEG recording and analysis were performed as described previously.[50,51] EEG and EMG signals were first amplified and filtered (EEG, 0.5–25 Hz; EMG, 20–200 Hz). All signals were digitized at 128 Hz and collected with Vital Recorder software (Kissei Comtec, Nagano, Japan). The raw EEG signal was passed through band-pass filters, which allowed the following frequency bands to be separated and displayed individually on four additional channels: delta (0.5–4 Hz), theta (4–8 Hz), alpha (8–12 Hz), and beta (12–20 Hz). The average peak-to-peak amplitude was automatically computed for each frequency band by SleepSign software. Absolute power spectra of the EEG signals were computed every 4 s from 0–25 Hz in steps of 0.25 Hz. For sleep amount analysis (conducted by SleepSign according to standard criteria[52,53]). All scoring was automatic based on EEG and EMG waveforms in 4 s epochs. We defined wakefulness as desynchronized EEG and high levels of EMG activity, NREM sleep as synchronized, high-amplitude, low-frequency (0.5–4 Hz) EEG signals in the absence of motor activity, and REM sleep as having pronounced theta like (6–8 Hz) EEG activity and muscle atonia. Vigilance states assigned by SleepSign (Kissei Comtec, Nagano, Japan) were examined visually and manually corrected after automatic scoring.

Neuropathic pain model and measurement of mechanical allodynia

Under anesthesia, mice received partial sciatic nerve injury (PSNL) and sham operation. Briefly, the right sciatic nerve was exposed and one-third to half of the nerve trunk was tightly ligated using a 6–0 silk suture. For the sham operation, the nerve was exposed without ligation. PSNL or sham mice were placed in separate home cages during the recovery period. and mechanical allodynia was measured as the hind paw-withdrawal response to von Frey-hair stimulation. The paw was touched with one of series of 8 von Frey filaments with logarithmically incremental hair stiffness (0.07, 0.16, 0.4, 0.6, 1.0, 1.4, 2.0, and 4.0 g). The von Frey filament was pressed perpendicular to the plantar surface with enough force to cause slight buckling, and was held for an additional 6 to 8 seconds. Stimuli were presented after various intervals (several seconds). Clear paw withdrawal, shaking, or licking was considered nociceptive responses. The hair force was increased or decreased according to the response. Ambulation was considered an ambiguous response, and in such cases, the stimulus was repeated.

Immunohistochemistry

For immunostaining of c-Fos and mCherry, mice were deeply anesthetized with 4% isoflurane and then perfused intracardially with 20 mL phosphate-buffered saline followed by 40 mL 4% paraformaldehyde (PFA). Brains were post-fixed for 24 h in 4% PFA and then transferred to 30% sucrose in PB at 4°C until they sank. Coronal sections (30 μm) were cut on a freezing microtome (CM1950, Leica, Germany). The floating sections were washed in PBS and incubated with a rabbit polyclonal antibody against c-Fos (1:5,000 dilution; Millipore) in PBS with 0.3% Tween-20 (PBST) for 48 h at 4°C on an agitator. After washing, sections were incubated with a 647-donkey anti-rabbit secondary antibody solution (1:1000) in 0.1% PBST for 2 h at 24 °C. For biocytin staining after whole-cell patch-clamp recordings, slices containing biocytin-loaded cells were fixed in 4% PFA and were then washed in PBS. Streptavidin conjugated to Alexa 647 (1:1000; Invitrogen Molecular Probes, USA) were used. Images were captured with Olympus confocal microscopy (FV3000, Olympus, Japan). Cell counting was performed on FIJI.

Electrophysiology

Brain slice preparation

Acute slices of the ACC and the DMS were prepared from D2R-EGFP mice or AAV virus-injected CaMKII-Cre mice. Mice were anesthetized with chloral hydrate and transcardially perfused with ice-cold cutting artificial cerebrospinal fluid (ACSF) containing (in mM): 213 sucrose, 2.5 KCl, 1.25 NaH2PO4, 26 $NaHCO_3$, 10 glucose, 2 Na-Pyruvate, 0.4 ascorbic acid, 3 MgSO4, 0.1 $CaCl_2$ (pH 7.3 when carbogenated with 95% O_2 and 5% CO_2). Brains were rapidly removed and sliced in coronal slices (300 μm thick) in ice-cold cutting ACSF using a vibrating microtome (VT 1200S, Leica). Slices containing the DMS or ACC were transferred to recording ACSF containing (in mM): 119 NaCl, 2.5 KCl, 1.25 NaH2PO4, 1 MgSO4, 2 CaCl2, 26 NaHCO3, and 25 Glucose. Slices were incubated at 32°C for 30 min and then stored at room temperature until used for patch clamp recordings (1–5 h). The extracellular ACSF was saturated with 95% O2/5% CO2 to maintain oxygenation and a pH ~7.435.

Whole-cell recordings ex vivo

Slices were visualized using a combination of fluorescence and infrared differential interference contrast (IR-DIC) video microscopy using a fixed-stage upright microscope (BX51WI, Olympus) equipped with a water immersion lens (40×/0.8 W) and an IR-sensitive CCD camera (IR1000, DAGE MTI). The recording chamber was superfused with carbogen-saturated warm (30–32°C) ACSF at a flow rate of 2–3 ml min^{-1}. Picrotoxin (100 μM) was added to block $GABA_A$ receptor-mediated IPSCs. mEPSCs were measured in voltage clamp at a holding potential of −70 mV and in the presence of 500 nM tetrodotoxin (TTX, to block voltage-gated sodium currents) and 25 μM d-(-)−2-amino-5-phosphonopentanoic acid (d-APV, to block NMDA receptor EPSCs). All drugs were dissolved in ACSF. Series resistance (Rs) compensation was not used. Therefore, cells with Rs changes over 25% were discarded.

Recordings were conducted in the cell-attached or whole-cell configuration using a Multiclamp 700B amplifier (Molecular Devices), a Digidata 1440A interface and Clampex 10.3 software (Molecular Devices). Optical stimulation was delivered to slices via an optical fiber (200 μm core, Thorlabs, Newton, USA) coupled to a 470 nm diode-pumped solid-state continuous-wave laser system (OEM Laser Systems Salt Lake City, USA). Stimulation consisted of either a single 1 ms pulse or trains of 1 ms pulses delivered at 10 Hz. The output of the laser was <2 mW. Recording electrodes (3–7 MΩ) were filled with an internal solution consisting of (in mM): 105 potassium gluconate, 30 KCl, 4 ATP-Mg, 10 phosphocreatine, 0.3 EGTA, 0.3 GTP-Na, 10 HEPES (pH 7.3, 295–310 mOsm). The internal solution also contained 0.2% biocytin. For mEPSCs and NMDAR/AMPAR ratio recording, electrodes (3–7 MΩ) filled with 120 CsMeSO4, 15 CsCl, 8 NaCl, 10 HEPES, 0.2 EGTA, 10 TEA-Cl, 4 Mg2+ATP, 0.3 NaGTP, and 5 QX-314 were used. Random recordings were obtained from neurons in the dorsal medial striatum expressing eGFP and from neurons in the region of the ACC expressing mCherry. MSN electrophysiological properties closely resembled those reported in earlier studies, including the presence of a slow ramping subthreshold depolarization in response to low-magnitude positive current injections, a hyperpolarized resting potential, inward rectification, and prominent spike after-hyperpolarization. MSNs were also characterized by a small to medium cellular body size (10–15 μm in diameter) and a radially oriented large dendritic tree covered by spines, confirmed by posthoc biocytin staining. To record evoked action potential firings, current injection steps were generated using Clampex software (Molecular Devices). After the cells had stabilized for 3 minutes and then the range of 0 to +400 pA, 50 pA increments/steps were chosen to elicit action potential spikes in DMS neurons.

For long-term potentiation (LTP) and paired-pulse ratio (PPR) experiments using electrical stimulation, a tungsten bipolar electrode (WPI) was placed in layer V/VI of the ACC close to the callosum, AMPAR-mediated EPSCs were induced by repetitive stimulations at

0.5 Hz, and neurons were voltage-clamped at -70 mV. Picrotoxin (100 μM) was always present to block $GABA_A$ receptor-mediated inhibitory synaptic currents in all experiments. The amplitudes of eEPSCs were adjusted to between 50-150 pA to obtain a baseline. Paired pulse ratio with a 50-ms interstimulus interval was recorded before the LTP recording. Recordings were rejected if input resistance changed by more than 30% during recordings. After 10 min of recording stable responses, high-frequency stimulation (HFS: 4 trains of stimuli spaced at 10-s intervals, with each train containing bursts of 100 spikes at 100 Hz) was delivered. Summary LTP graphs were constructed by normalizing data in 30s epochs to the mean value of the baseline EPSCs.

For recording the AMPA receptor/NMDA receptors current ratios, EPSCs of DMS D1/D2R-MSNs were evoked by ChR2 stimulation using 473-nm light pulses (1 ms, 0.33-Hz LED, CoolLED), and were recorded in voltage clamp. The AMPA-mediated currents were recorded at a holding potential of -70 mV, and the NMDAR-mediated current was recorded at +40 mV.

In vivo calcium imaging and analysis

To record the calcium dynamic in ACC PNs, we first injected AAV-DIO-GCaMP6f into the ACC of CaMKII-Cre mice. After 2 weeks, a gradient refractive index (GRIN) lens (length: 2 mm, core 6 diameter: 0.6 mm) was implanted in the same position under the monitor of the imaging software (Inscopix, nVista 3.0) to display incoming fluorescence. After a week, the recording was taken by a single photon miniature fluorescence microscope (Inscopix nVista) attached to a baseplate positioned atop the GRIN lens to get the best focal plane. Both the GRIN lens and baseplate were fixed to the skull with dental cement. All imaging sessions were conducted in mice freely behaving in their home cage. At the session onset, the microscope was attached to a skull-mounted baseplate and mice were rested in their home cage for 20 min. Calcium images were recorded with the nVista® software (Inscopix, Inc) at a sample rate of 10 frames s^{-1}, and under 10% LED blue radiance power. Continuous imaging periods lasted 10 min for each mouse in light phase 07:00-09:00 and dark phase 19:00-21:00, and the same mouse was repeated recording 7 days after PSNL. The same PSNL mice were treated by diazepam (6 mg/kg), gabapentin (100 mg/kg) and morphine (1 mg/kg) with an interval of 3 days to wash out. Raw imaging data were processed using the Inscopix Data Processing software (Inscopix DPS®, Inc.). AUC for each cell was calculated. Only PNs had calcium activity before and after PSNL surgery were compared, and activated PNs had at least a 20% increase in AUC, while deactivated PNs have a 20% decrease.

Locomotion in open field test

The open field test apparatus was a Plexiglas-squared arena (45 × 45 cm^2) with gray walls (40 cm high) and an open roof, which was located in a sound-attenuated and dimly illuminated room. Mice were gently placed in the center of the field, and movement was recorded for 5 min with a video-tracking system. Locomotion was analyzed by EthoVision XT (Noldus).

QUANTIFICATION AND STATISTICAL ANALYSIS

Data are expressed as the mean ± standard error of the mean (SEM). No statistical methods were used to pre-determine sample sizes but our sample sizes are similar to those reported in previous publications.[50,51,54–57] Animals or data points were not excluded and each experiment was repeated 2 times. Data analysis was performed blinded to the conditions of the experiments. Statistical significance was assessed using two-tailed Student's *t*-tests to compare two groups. One-way, two-way, or repeated-measures ANOVAs were used to compare multiple groups, with pairwise comparisons made using a Tukey post-hoc test. Statistical details can be found in figure legends. A two-tailed P-value < 0.05 was considered statistically significant. All data were analyzed using Prism 8 software.